Relaxation breakdown and resonant tunneling in ultrastrong-coupling cavity QED

Daniele De Bernardis [*]

Pitaevskii BEC Center, CNR-INO and Dipartimento di Fisica, Università di Trento, I-38123 Trento, Italy

We study the open relaxation dynamics of an asymmetric dipole that is ultrastrongly coupled to a single electromagnetic cavity mode. By using a thermalizing master equation for the whole interacting system we derive a phase diagram of the Liouvillian gap. It emerges that the ultrastrong coupling inhibits the system's relaxation toward the equilibrium state due to an exponential suppression of the dipole tunneling rate. However, we find that polaronic multiphoton resonances restore fast relaxation by a cavity-mediated dipole resonant tunneling process. Aside from the numerical evidence, we develop a fully analytical description by diagonalizing the Rabi model through a generalized rotating-wave approximation, valid in the so-called polaron frame. The relaxation physics of such ultrastrong-coupling systems is then reduced to a multiphoton polaron version of the standard textbook dressed states picture. At the end we discuss an extension to a multiwell dipole that can set the basis of a cascaded resonant tunneling setup in the ultrastrong coupling regime.

I. INTRODUCTION

Relaxation from a metastable state toward equilibrium is a central problem in many branches of physics, such as chemical reactions, radiooactive decay, and electronic transport, to name a few [1]. The energy barrier separating a local minimum from the stable equilibrium, i.e., the activation barrier of chemical reactions [2], can be overcome by thermal fluctuations, for which, after an initial absorption of energy from the bath, the system is kicked out the metastable state, rolling down to its absolute equilibrium state and releasing the energy excess. When the temperature is too small to kick the system over the metastable energy barrier, relaxation is then dominated by the *tunnel effect* (or quantum tunneling), which is one of the first surprising consequences of the quantum theory [3].

Following the hand-waving intuition that quantum fluctuations replace thermal ones in kicking the system out of the metastability, one might speculate that including in these systems a supplemental quantum reservoir could sensibly alter the tunneling dynamics. The work of Leggett *et al.* on tunneling systems coupled to an environment [4,5] has shown that this is actually the case, and tunneling can be sensibly changed as a function of the environment parameters. Since for most systems the natural environment is provided by the electromagnetic radiation, here quantum tunneling is crossing its path with another fundamental concept of quantum physics: the nonempty vacuum of quantum electrodynamics (QED) [6], rising the question: can vacuum fluctuations of the electromagnetic field affect tunneling and relaxation in material systems?

Experiments have shown strong suggestions that the answer may be positive, and that the electromagnetic vacuum of a resonant cavity could have a major role in chemical reaction and electronic transport where important differences are observed when molecules, atoms or electrons couple strongly or ultrastrongly to such a extreme resonant electromagnetic environment [7–10].

All these exciting observations have stimulated multiple theoretical debates in various communities, opening new research lines such as: polaritonic chemistry [11–13], cavity QED control of electronic transport in mesoscopic devices or in quantum Hall systems [8,14], cavity QED modification of ferromagnetism, ferroelectricity, and superconductivity [15–20], and their out-of-equilibrium extensions [21–28], all with the general aim to explore and understand up to which degree the quantum vacuum of cavity QED can be a resource to modify and control properties of matter [29–32].

However, in the community there is still not a full consensus about the origin, validity, and interpretation of these theories and their relation with the actual experimental evidence [33–36], suggesting that more research and additional examples are needed to completely clarify these physical mechanisms.

In this article we explicitly address the problem of how the electromagnetic vacuum of ultrastrong-coupling cavity QED can affect the relaxation toward equilibrium of a polarizable material. In order to isolate every different effect we consider a simple paradigmatic setup: an asymmetric double-well dipole in a single-mode resonant cavity. Its low-energy dynamics can be approximated to the *quantum Rabi model*, which is the simplest theoretical framework with which to study light-matter interactions. We complete the description of the model including two basic dissipative mechanisms: Ohmic cavity dissipation and dipole radiative losses. Under these circumstances the system's relaxation is described through a thermalizing master equation valid for arbitrary light-matter coupling values, whose steady state is the correct thermal equilibrium state. From the spectral gap λ of its Liouvillian operator we derive a phase diagram describing how relaxation toward equilibrium is modified by the coupling to the cavity.

---
[*]daniele.debernardis@ino.cnr.it

The intuition arising from all recent works regarding thermalization and transport in cavity QED would suggest that the coupling with the cavity always favors and accelerates the relaxation properties of the system. However, here we show that an increasing light-matter coupling strength from the strong to the ultrastrong coupling regime exponentially suppresses the relaxation rate of the dipole, being a prototype for the so-called localization transition in the spin-boson model [5]. The cavity-induced inhibition of the dipole relaxation is restored only due to the occurrence of polaronic multiphoton resonant tunneling processes, in very close analogy to Franck-Condon physics describing electron tunneling assisted by vibrational transitions [37–40]. After showing that this mechanism is already observable in current experimental platforms such as superconducting circuits we comment on the possible consequence for cavity-assisted quantum transport and cascaded ultrastrong-coupling setups with multiwell dipoles.

Differently from previous studies [21–23], we exploit a generalized rotating-wave approximation of the Rabi model from which we analytically derive the transition rates of the master equation in the ultrastrong coupling regime. From this calculation we obtain a complete and simple picture of how relaxation and thermalization work in terms of polaronic dressed states, valid in the ultrastrong coupling regime.

The article is organized as follows. In Sec. II we introduce the physical system and its approximated description in terms of the asymmetric quantum Rabi model. By considering the Liouvillan gap of its open dynamics, in Sec. III we study how the ultrastrong coupling regime changes the relaxation and thermalization rate. By using a generalized rotating-wave approximation to diagonalize the Rabi model we explicitly show an exponential slow-down of the system's relaxation due to the ultrastrong coupling regime. In Sec. IV we show that the fast relaxation can be restored by a cavity-assisted multiphoton resonant tunneling process. Exploiting again the generalized rotating-wave approximation we develop the discussion in terms of multiphoton polaron dressed states. In Sec. V we extend this setup to the extended Dicke model leading to a cascaded resonant tunneling device. Finally, in Sec. VI we draw our conclusions.

II. MODEL

We consider the paradigmatic cavity quantum electrodynamics (cQED) setup described in Fig. 1(a), where a single electrically polarizable object (a dipole) is placed into the planar capacitor of a resonant LC circuit. This simple toy model is able to reproduce most of the features of cQED in all various coupling regimes and is particularly important in giving a simple and intuitive description of many solid-state or circuit cQED setups relevant for experiment in the ultrastrong coupling (USC) regime in the GHz or THz range [15,41–44]. The system cavity QED Hamiltonian is given by the so-called *asymmetric Rabi model* ($\hbar = 1$)

$$H_{\mathrm{cQED}} \approx H_{\mathrm{Rabi}} = \omega_c a^\dagger a + \omega_d s_z + \epsilon s_x + g(a + a^\dagger)s_x, \quad (1)$$
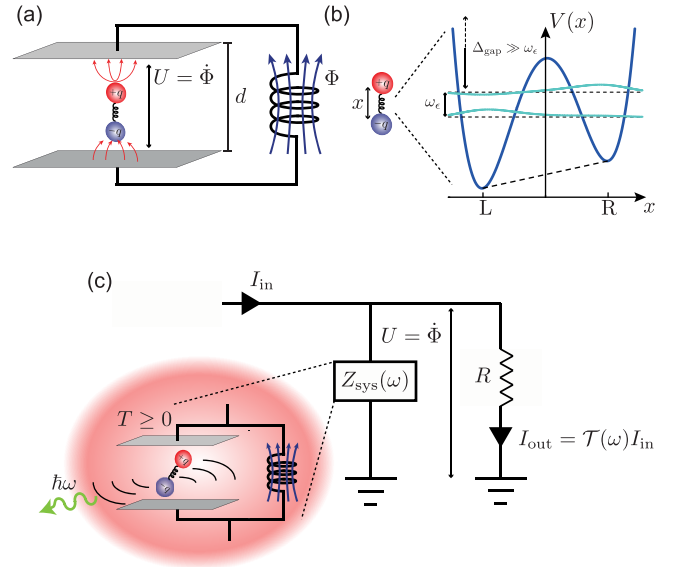

FIG. 1. (a) Cavity QED system. The cavity is modeled as an LC circuit, where the inductor magnetic flux Φ takes the role of the dynamical variable of the electromagnetic field, usually given by the vector potential $\vec{A}$. The dipole inside the capacitor couples to the voltage drop $U = \dot{\Phi}$ between the plates, separated by the distance d. (b) The dipole is described as a particle in a tilted double-well potential. The position x represents the displacement between the two charges q, $-q$, such that the dipole moment is qx. When the central well of the potential is large enough the system is approximated by only the two lowest levels (two-level approximation; see Appendix A). (c) Open-system schematic view. The cavity QED system can be interpreted as an element of a dissipative circuit.

where a is the annihilation operator of a cavity photon with frequency ω_c. The pseudospin operators $s_{x,z}$ are linked, respectively, to the dipole moment x and the dipole internal energy through the two-level approximation, ω_d is the dipole lowest transition frequency, and ϵ is the dipole asymmetry (which breaks the $\mathbb{Z}_2$ symmetry of the Rabi model). The dipole eigenstates are also asymmetric with frequencies $\pm \omega_\epsilon/2 = \sqrt{\omega_d^2 + \epsilon^2}/2$, and this picture holds until the two-level subspace is well separated in energy from the rest of the spectrum; see Fig. 1(b) for a schematic view. Finally, g is the light-matter interaction strength due to the dipole coupling to the cavity. A complete derivation of the model is presented in Appendixes A and B.

As schematically shown in Fig. 1(c), the system dissipates energy mainly in two external environments: a resistive element (or transmission line) for the cavity, and free-space radiative modes for the dipole. The full system dynamics is thus obtained from the contribution of three Liouvillian superoperators

$$\partial_t \rho = \mathcal{L}_H(\rho) + \mathcal{L}_c(\rho) + \mathcal{L}_{\mathrm{dip}}(\rho), \quad (2)$$

where

$$\mathcal{L}_H(\rho) = -i[H_{\mathrm{Rabi}}, \rho] \quad (3)$$

generates the coherent time evolution, while the cavity and dipole dissipative dynamics are given by

$$
\mathcal{L}_{c/\mathrm{dip}}(\rho) = \sum_{n<m} [1 + N_T(\omega_{mn})] \Gamma_{nm}^{c/\mathrm{dip}} D(|n\rangle\langle m|, \rho)
$$
$$
+ \sum_{n<m} N_T(\omega_{mn}) \Gamma_{nm}^{c/\mathrm{dip}} D(|m\rangle\langle n|, \rho). \quad (4)
$$

Here $D(c, \rho) = c\,\rho\,c^\dagger - \frac{1}{2}[c^\dagger c, \rho]_+$ is the usual dissipator super-operator [45] ($[\cdot, \cdot]_+$ is the anticommutator), and $N_T(\omega) = 1/\{\exp[\omega/(k_B T)] - 1\}$ is the bosonic thermal population, where k_B is the Boltzmann constant. The transition rates of the relaxation dynamics are given by

$$
\Gamma_{nm}^c = J_{\mathrm{Ohm}}(\omega_{mn}) |\langle n|c_{nm}^c|m\rangle|^2 = \gamma \frac{|\omega_{mn}|}{\omega_c} |\langle n|a - a^\dagger|m\rangle|^2,
$$

$$
\Gamma_{nm}^{\mathrm{dip}} = J_{\mathrm{rad}}(\omega_{mn}) |\langle n|c_{nm}^{\mathrm{dip}}|m\rangle|^2 = \kappa \frac{|\omega_{mn}|^3}{\omega_d^3} |\langle n|s_x|m\rangle|^2, \quad (5)
$$

where $\omega_{mn} = \omega_m - \omega_n$ is the difference between the eigenfrequencies of the Rabi Hamiltonian in Eq. (1), while $J_{\mathrm{Ohm}}(\omega) = \gamma \omega/\omega_c$ is the spectral density of the resistance (cavity bath), which is Ohmic, with photon loss rate γ, and $J_{\mathrm{rad}}(\omega) = \kappa \omega^3/\omega_d^3$ is the spectral density of the radiative modes (dipole bath), which is super-Ohmic with dipole decay rate κ. Notice that a different choice for these spectral densities does not change our main conclusions, as long as the spectral densities are Ohmic or super-Ohmic. See Appendix E for important details regarding the modeling of dissipation.

It is then easy to verify that the steady state of such a defined master equation is correctly given by the thermal density matrix $\rho(t = +\infty) = \rho_T = e^{-H_{\mathrm{Rabi}}/(k_B T)}/\mathcal{Z}$, where $\mathcal{Z} = \mathrm{Tr}[e^{-H_{\mathrm{Rabi}}/(k_B T)}]$.

III. RELAXATION REGIMES OF CAVITY QED

In this section we will explore the combined effect of light-matter coupling g and dipole asymmetry ϵ on the open relaxation dynamics of the system. For the sake of simplicity, through the whole paper we focus only on the relevant dipole-cavity resonant case where $\omega_c = \omega_d$.

A. Zero temperature Liouvillian gap

To have a first indication about the relaxation properties of the system we consider the Liouvillian gap $\lambda = \mathrm{Re}[\lambda_1]$ [46–48], obtained from the spectrum $\{\lambda_n\}$, $n = 0, 1, 2 \ldots$, of the total Liouvillian operator $\mathcal{L} = \mathcal{L}_H + \mathcal{L}_c + \mathcal{L}_{\mathrm{dip}}$ defined from Eq. (2) [49]. This quantity provides the slowest relaxation rate of the system, describing the long-time evolution of the system, for which before reaching its thermal steady state the density matrix decays as [46,48]

$$
\lim_{t \to \infty} \rho(t) \approx \rho_T + \rho_1 e^{\lambda t}. \quad (6)
$$

It is worth noticing that using the Liouvillian gap to characterize the relaxation toward equilibrium is not always straightforward and may cause problems in more complex many-body systems [50]. We will see that in our case it works without problems or ambiguities, correctly matching the expected physical predictions and giving a correct and
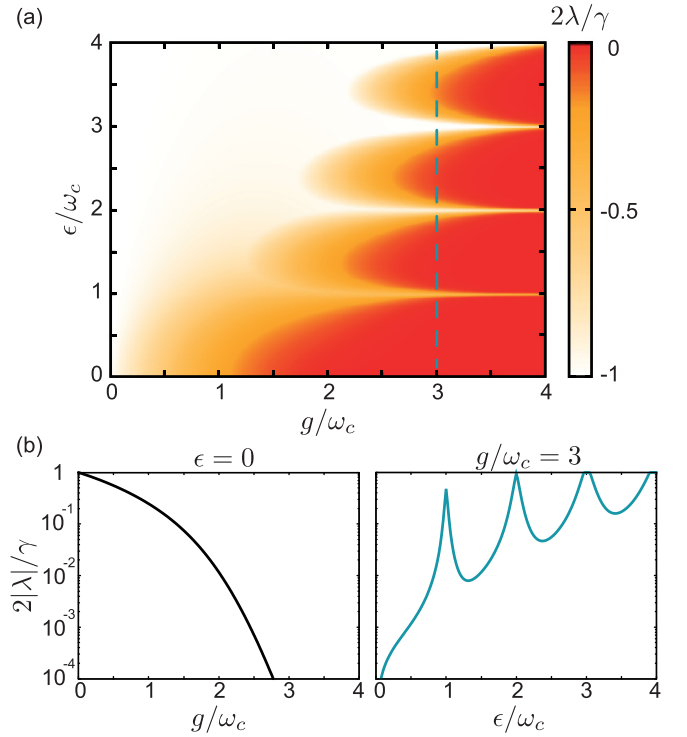

FIG. 2. (a) Phase diagram of the Liouvillian gap λ as a function of the light-matter coupling g and the dipole asymmetry ϵ. Parameters: $\gamma = \kappa/4 = 0.05\omega_c$, $\omega_d = \omega_c$. (b) A cut of the phase diagram at $\epsilon = 0$ as a function of the light-matter coupling g, in logscale. (c) A cut of the phase diagram at $g/\omega_c = 3$ as a function of the dipole asymmetry ϵ, in logscale.

clear picture of how relaxation works as a function of our control parameters (g, ϵ).

We consider only the zero-temperature case $T = 0$, which is the relevant case for superconducting cavity QED setups [51]. The same picture holds also for finite temperature, provided that $k_b T \lesssim \hbar\omega_c, \hbar\omega_d$, where k_b is the Boltzmann constant. When the temperature grows larger, and $k_b T > \hbar\omega_c$ USC effects are pushed to much larger light-matter coupling values [52].

In Fig. 2(a) we show the Liouvillan gap as a function of the light-matter coupling and the dipole asymmetry, $\lambda(g, \epsilon)$. At small light-matter coupling $g \sim 0$, the effect of increasing ϵ is to progressively rotate the dipole eigenstates from the s_z basis to the s_x basis, decreasing the value of the matrix element in the dipole transition rate in Eq. (5). However, the vanishing matrix element is compensated by the increasing energy difference between the dipole levels, giving a larger contribution from the radiative spectral density of the bath, $J_{\mathrm{rad}} \sim \omega^3$. This can be seen by explicitly computing the dipole transition rate at $g = 0$ using the bare uncoupled dipole states in Eq. (A4), for which we have

$$
\Gamma_{\mathrm{LR}}^{\mathrm{dip}} = \frac{\kappa}{4} \left(1 + \frac{\epsilon^2}{\omega_d^2}\right)^{3/2} \cos\left[\tan^{-1}\left(\frac{\epsilon}{\omega_d}\right)\right]
$$

$$
= \frac{\kappa}{4} \sqrt{1 + \frac{\epsilon^2}{\omega_d^2}}. \quad (7)
$$

In the specific case $\kappa = 4\gamma$ this rate is always larger than the bare photon loss set by γ which becomes the slowest relaxation timescale, and so we have $\lambda = -\gamma/2$. In such conditions, the Liouvillian gap does not show any structure as long as the light-matter coupling remains small. It is worth noticing that replacing the super-Ohmic radiative spectral density with an Ohmic spectral density would give too slow of an increase of the decay rate as a function of the transition frequency to compensate for the effect of the vanishing matrix element of the dipole transition rate. As a result we would have that $(\Gamma_{\mathrm{LR}}^{\mathrm{dip}})^{\mathrm{Ohm}} = \kappa/(4\sqrt{1 + \epsilon^2/\omega_d^2})$, and so the overall relaxation rate would decrease as a function of ϵ at very weak coupling $g/\omega_c \simeq 0$ to then increase again at slightly larger coupling. In this case the Liouvillian gap λ would exhibit a different structure as a function of (g, ϵ), in the weak-coupling limit. Giving rid of this weak-coupling feature only considering a radiative bath (and thus a super-Ohmic spectral density) for the dipole highlights the effect of the USC, making this choice particularly meaningful.

In the USC regime, $g/\omega_c \gg 1$, for small dipole asymmetry $\epsilon \simeq 0$, the Liouvillian gap goes to zero monothonically with an exponential behavior $\lambda \sim -\exp[-g/\omega_c]$, as is clearly visible from Fig. 2(b). Increasing the dipole asymmetry, ϵ, we observe the emergence of lobes where the Liouvillian gap approaches zero $\lambda \sim 0$, separated by a narrow region where relaxation is partially restored and $\lambda \sim -\gamma/2$. This is shown in Fig. 2(c), where we fixed $g/\omega_c = 3$ and we plot λ as a function of ϵ. Quite surprisingly, these narrow gaps between the lobes appear only when $\epsilon \simeq \omega_c \times k$, where $k = 1, 2, 3, \ldots$ is an integer number. Moreover this lobular structure is present also in the higher Liouvillian eigenstates, suggesting important physical consequences for the system.

B. Relaxation breakdown in the USC regime

The thermalization exponential slow-down pointed out by the spectral analysis of the Liouvillian $\mathcal{L}$ can be understood as an interplay between the USC spectral properties and transition rates in Eq. (5) (due to the dressing of the jump operators in the USC regime [53,54]; see Appendix D). Here we analyze in detail the symmetric case, when $\epsilon = 0$, which will provide the basic tools to understand the whole phase diagram of Fig. 2(a).

We start by transforming the original Rabi Hamiltonian through the unitary transformation $U_{\mathrm{pol}} = \exp[g/\omega_c(a - a^\dagger)s_x]$, and obtaining the *Rabi polaron* Hamiltonian ($\hbar = 1$)

$$\tilde{H}_{\mathrm{Rabi}} = \omega_c a^\dagger a + \epsilon s_x + \frac{\omega_d}{2}[\mathcal{D}(g/\omega_c)\tilde{s}_+ + \mathcal{D}^\dagger(g/\omega_c)\tilde{s}_-].$$

$$(8)$$

Here $\tilde{s}_\pm = s_z \pm i s_y$ are the raising and lowering operators along the s_x axis, while $\mathcal{D}(g/\omega_c) = \exp[g/\omega_c(a - a^\dagger)]$ is the usual displacement operator.

Since both cavity and dipole dissipative operators are unaffected by the polaron transformation $U_{\mathrm{pol}}(a - a^\dagger)U_{\mathrm{pol}}^\dagger = (a - a^\dagger)$, $U_{\mathrm{pol}}s_x U_{\mathrm{pol}}^\dagger = s_x$, the general master equation defined in Eqs. (2), (3), and (4) is still valid, with the only difference that the eigenstates $|n\rangle, |m\rangle$ appearing in the transition rates in Eq. (5) are now replaced with the eigenstates of the Rabi polaron Hamiltonian in Eq. (8).
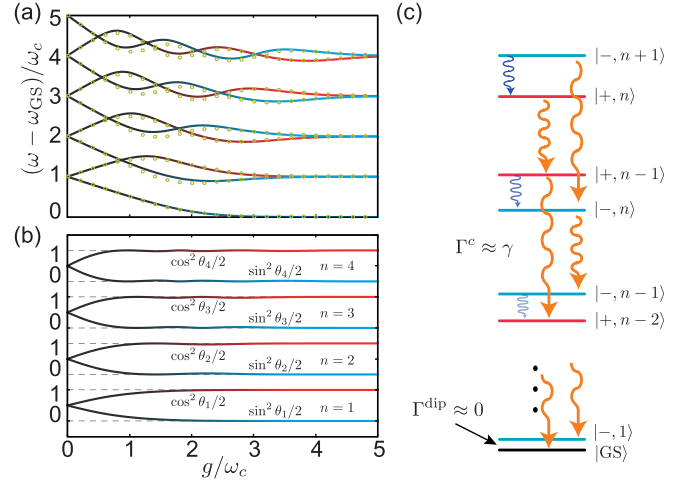

FIG. 3. (a) Spectrum of the Rabi model as a function of the light-matter coupling g at fixed $\epsilon = 0$. The solid lines are the result of full diagonalization, and the red and blue are meant only to match the color code in (c). The yellow dots are given by the analytic (F6) in Appendix F. (b) $\cos\theta_n/2$, $\sin\theta_n/2$ given by Eq. (F8) for each n block as a function of the light-matter coupling g. (c) Scheme of the relaxation mechanism. The cavity relaxes jumping mainly between $++$ or $--$ dressed states, while for the dipole it is mainly between $+-$ states. The orange curly arrows represent the decay of the photon from an upper state to a lower one, while the blue curly arrows represent the decay of the dipole. In the USC limit the dipole does not relax anymore. Parameters: $\epsilon = 0$, $\omega_c = \omega_d$.

As reported in [55] and detailed in Appendix F, the polaron Rabi Hamiltonian supports a generalized rotating-wave approximation (gRWA) and thus follows the structure of the Jaynes-Cummings model, with the approximated conservation of the polaron excitation number $\hat{N}_{\mathrm{exc}}^z = a^\dagger a + s_z$. Its eigenstates are then given by the usual dressed states

$$|+, n\rangle = \cos\frac{\theta_n}{2}|\downarrow, n\rangle + \sin\frac{\theta_n}{2}|\uparrow, n - 1\rangle,$$
$$|-, n\rangle = -\sin\frac{\theta_n}{2}|\downarrow, n\rangle + \cos\frac{\theta_n}{2}|\uparrow, n - 1\rangle,$$

$$(9)$$

where θ_n is given in Appendix F. The ground state of the system is simply the uncoupled vacuum state

$$|\mathrm{GS}\rangle = |\downarrow, 0\rangle.$$

$$(10)$$

To appreciate the quality of this approximation, in Fig. 3(a) we compare the spectrum obtained from the exact diagonalization (solid lines) and from the gRWA analytical formula reported in Appendix F (yellow dots), from which is quite clear that the gRWA gives very good results. Relaxation can then be understood from the dressed state perspective [56], and in Appendix G we explicitly compute the transition rate in Eq. (5).

From the explicit expression for the Hopfield coefficients $\sin, \cos$ (presented in Appendix F), we find that in the infinite-

coupling limit

$$\lim_{g/\omega_c \to \infty} \cos \frac{\theta_n}{2} = 1,$$

$$\lim_{g/\omega_c \to \infty} \sin \frac{\theta_n}{2} = 0. \quad (11)$$

This is clearly shown in Fig. 3(b), where we plot the Hopfield coefficient analytically computed through the gRWA for a few lowest eigenstates. Using this observation together with the matrix element computed in Appendix G we can build the transition rates in Eq. (5), arriving at the conclusion that the only non-negligible transitions in the USC regime are

$$\lim_{g/\omega_c \to \infty} \Gamma^c_{(+,n)(+,n-1)} = \gamma \frac{\omega_{+,n} - \omega_{+,n-1}}{\omega_c} \approx \gamma,$$

$$\lim_{g/\omega_c \to \infty} \Gamma^c_{(-,n)(-,n-1)} = \gamma \frac{\omega_{-,n} - \omega_{-,n-1}}{\omega_c} \approx \gamma,$$

$$\lim_{g/\omega_c \to \infty} \Gamma^{\text{dip}}_{(-,n)(+,n-1)} = \kappa \left(\frac{\omega_{-,n} - \omega_{+,n-1}}{\omega_c} \right)^3 \approx 0. \quad (12)$$

The fact that the dipole transition rate goes to zero $\Gamma^{\text{dip}}_{(-,n)(+,n-1)} \approx 0$ follows from the approximate degeneracy of the states $|-,n\rangle, |+, n-1\rangle$ in the USC limit, for which $\omega_{-,n} - \omega_{+,n-1} \approx 0$, while $\omega_{+,n} - \omega_{+,n-1} \approx \omega_{-,n} - \omega_{-,n-1} \approx \omega_c$.

Here we realize that the USC Liouvillian gap suppression observed in Figs. 2(a) and 2(b) is due to only a suppression of the dipole transition rates only, while the cavity transition rates return to their bare uncoupled values when the USC regime is reached. In the infinite coupling limit the exponential slowdown becomes a proper cavity-induced breakdown of the relaxation of the dipole, resulting in a localization transition similar to what happens in the so-called spin-boson model [5]. The schematic representation of the remaining relaxation channels is shown in Fig. 3(c). It is important to stress that what described above holds only in the infinite coupling limit, and for finite values of the light-matter coupling g, the long-time dynamics is always given by the finite Liouvillian gap, for both the dipole and the cavity. However, if we consider the relaxation of a single photon (in the polaron frame) in the USC regime, initializing the system in the state $\rho_{0,\text{ph}} = |1_{\text{ph}}, \downarrow\rangle\langle 1_{\text{ph}}, \downarrow|$ we observe a transient dynamics where the system relaxes as a bare cavity photon as $\exp[-\gamma t]$, and arriving progressively closer to the equilibrium state before entering in the long-time dynamics settled by the suppressed Liouvillian gap. On the other hand, initializing the state in a pure dipole excitation (in the polaron frame) $\rho_{0,d} = |0_{\text{ph}}, \uparrow\rangle\langle 0_{\text{ph}}, \uparrow|$, the system enters almost immediately in the long-time dynamics, remaining frozen there. This is well seen from the time evolution of the infidelity with respect to the thermal state (or, at $T=0$, the ground state) $1 - \mathcal{F} = 1 - \text{Tr}[\sqrt{\sqrt{\rho(t)} \rho_T \sqrt{\rho(t)}}]$ [49], which is shown in Fig. 4. In particular in Figs. 4(a) and 4(b) we show, for comparison, the time evolution at weak and intermediate coupling. It is well seen the slower relaxation at higher coupling, but the two different states still decay to the ground state in a similar way. In Fig. 4(c) on the contrary there is a strong asymmetry in the dipole and photon state decay, and it is clear that asymptotically a single polaron photon decays with its bare decay rate,
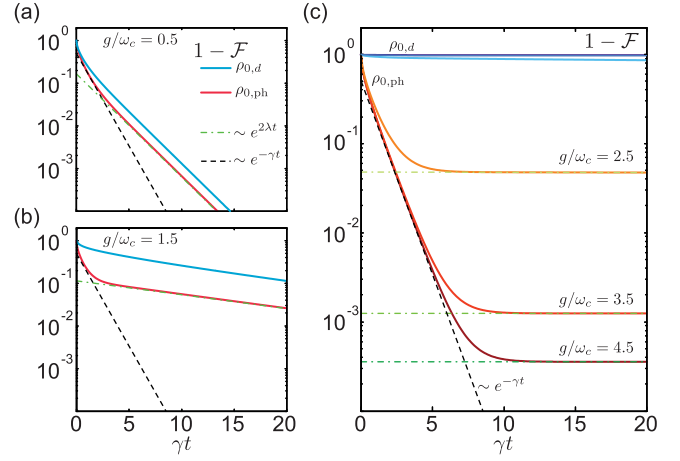

FIG. 4. Infidelity time evolution. (a), (b) Weak and intermediate coupling regime, the infidelity is calculated starting with the initial density matrix $\rho_{0,d}$ (blue solid line) and $\rho_{0,\text{ph}}$ (red solid line). The black dashed line highlights the bare decay scaling $s_0 \exp[-\gamma t]$, while the green dot-dashed line marks the scaling given by the Liouvillian gap $s_0' \exp[2\lambda t]$ (s_0, s_0' are arbitrary offsets). The light-matter coupling is given in the panels. (c) USC regime, the infidelity is calculated starting with the initial density matrix $\rho_{0,d}$ (weak blue, middle blue, deep blue solid lines) and $\rho_{0,\text{ph}}$ (orange, red, dark red solid lines). For both initial state the couplings are $g/\omega_c = 2.5, 3.5, 4.5$ going from the lighter to the darker color. The middle blue and deep blue lines representing the infidelity starting from $\rho_{0,d}$ are almost overlapping and not well distinguishable. Parameters: $\omega_c = \omega_d, \epsilon = 0, \gamma = \kappa/4 = 0.1\omega_c, T = 0$.

while a polaron dipole excitation is completely frozen and does not decay. This behavior is not specific for the infidelity only, but it is common for most of the observables and states of this system.

This result can be physically interpreted from a polaronic perspective: the USC cavity vacuum heavily dresses the dipole with virtual photons, which inhibit its ability to tunnel from one side to the other of its double-well potential. Because of the radiative nature (but in the Ohmic case as well) of its dissipation mechanism, the dipole can loose energy moving only between the two wells (i.e., tunneling), and the faster it moves the stronger it dissipates. In this regime of heavy dressing by virtual-photon, tunneling becomes extremely slow and so it becomes the dipole's rate to release energy in the bath.

IV. USC MULTIPHOTON RESONANT TUNNELING

In this section we are going to explore more in detail the nature of the gaps between the relaxation-slowdown lobes in Fig. 2(a). In these narrow regions the system can relax, as it is almost unaffected by the USC suppression of tunneling described in the previous section. However, if we artificially remove the cavity dissipation, $\gamma = 0$, we see that these narrow gaps disappear. This suggests that the suppression of tunneling described above is still present for $\epsilon \neq 0$, but a new resonant mechanism appears, allowing the dipole to tunnel again by exchanging photons with the cavity. This effect is the cavity analogous of resonant tunneling in electronic setups interacting with vibrational degrees of freedom, and thus establishing

a connection between USC cavity QED and Franck-Condon physics in molecular-electronic setups [37,39,40].

After analyzing the relaxation properties from the spectral features of the system, as in the previous section, we show that the signature of this physics is also present in quantities that are not strictly related to relaxation and real-time dynamics, such as transmission spectra.

A. Diagonalization of the asymmetric Rabi Hamiltonian

As in the symmetric case $\epsilon = 0$, also the asymmetric Rabi model, $\epsilon \neq 0$ is approximately block-diagonal, as a consequence of the general form of the displacement operators. However, here the situation is more complicated, and we cannot find a unique formula that fits the whole spectrum for every (ϵ, g), but we can have analytic expressions valid only near each resonance.

We start by noticing that Eq. (8) is written in a form that calls for the gRWA, provided that the system has an *asymmetric resonance* $\epsilon \simeq \omega_c \times k$, with $k = 1, 2, \ldots$. Differently from the usual Jaynes-Cummings model, and the gRWA of the symmetric Rabi model, here we need to take the dipole basis as an eigenstate of s_x. Moreover, considering higher resonances at $\epsilon = \omega_c, 2\omega_c, 3\omega_c \ldots$ is well motivated by the fact that the displacement operator contains all powers of creation and annihilation operators, giving access to multiphoton processes with higher frequencies. This is indeed well seen considering the normal-order expansion [57]

$$\mathcal{D}(x) = e^{-x^2/2} \sum_{n,m=0} \frac{(xa^\dagger)^n}{n!} \frac{(-xa)^m}{m!}. \quad (13)$$

From this expression is also clear that the nonlinear interaction term in the polaron Hamiltonian in Eq. (8) is exponentially suppressed by the factor $\sim \omega_d e^{-g^2/(2\omega_c^2)}$. As a consequence, when

$$\epsilon, \omega_c > \omega_d e^{-g^2/(2\omega_c^2)} \quad (14)$$

the polaron light-matter interaction becomes perturbative, and we can adopt the gRWA. Notice that this correspond to keep only the terms $n < m$ with $\omega_c(m - n) \simeq \epsilon$ in Eq. (13), so, even if the interaction is perturbative, it is still multiphoton and thus highly nonlinear.

The asymmetric polaron Rabi Hamiltonian can then be approximately diagonalized around each k resonance by projecting it on the states $\{|\leftarrow, n\rangle, |\rightarrow, n - k\rangle\}$ and the ground state is simply given by $|GS\rangle \approx |\leftarrow, 0\rangle$. As for the symmetric case explained in Appendix F this treatment is equivalent to a quasidegenerate perturbation theory on a polaron interaction Hamiltonian

The Hamiltonian then can be expressed succinctly in a matrix form as the sum of 2×2 blocks

$$\tilde{H}_{\text{Rabi}}^k \approx \sum_{n=1}^{\infty} \frac{\omega_c k - \epsilon}{2} \sigma_x^{(n,k)} + \frac{\omega_d}{2} \mathcal{D}_{n\,n-k} \sigma_z^{(n,k)}$$
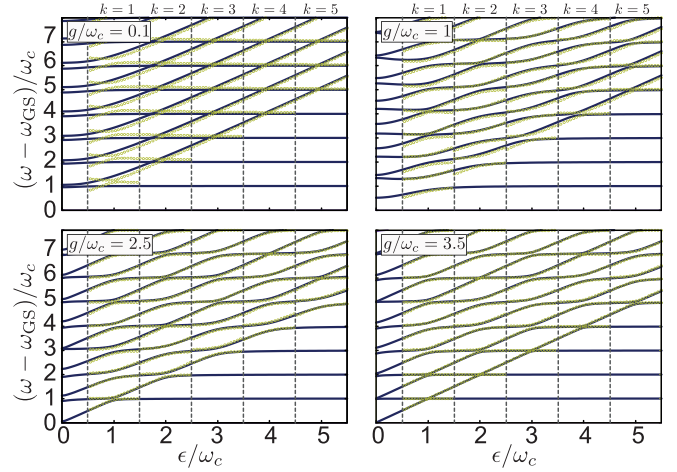$$+ \frac{2\omega_c n - \omega_c k}{2} \mathbb{1}_{(n,k)}, \quad (15)$$

FIG. 5. Spectrum of the Rabi model as a function of the dipole asymmetry ϵ for various $g/\omega_c = 0.1, 1, 2.5, 3.5$ light-matter couplings. The solid lines are the result of exact diagonalization, while the yellow dots are given by the analytical formula in Eq. (17). For $k > 1$ the yellow dots do not cover the lower lines because our approximation treats these eigenstates as a bare photon state for which the energy is trivially $n\omega_c$. To highlight the part of the spectrum where cavity and dipole are effectively coupled we do not put the yellow dots on these trivial eigenvalues. Parameters: $\omega_d = \omega_c$.

where $\sigma_{x,y,z}^{(n,k)}$ are the Pauli matrices for each $n = 1, 2, \ldots$ block for the k resonance, while

$$\mathcal{D}_{n\,n-k} = \frac{g^k}{\omega_c^k} e^{-\frac{g^2}{2\omega_c^2}} L_{n-k}^{(k)}\left(g^2/\omega_c^2\right) \sqrt{\frac{(n-k)!}{n!}} \quad (16)$$

is the $n, n - k$ matrix element of the displacement operator [57]. Here $L_m^{(l)}(x)$ is the special Laguerre polynomials. The excited eigenfrequencies are then given by

$$\omega_{k,n,\pm}^R = \omega_c\left(n - \frac{k}{2}\right) \pm \frac{1}{2}\sqrt{(\omega_c k - \epsilon)^2 + \omega_d^2 \mathcal{D}_{n\,n-k}^2}. \quad (17)$$

Since the displacement operator has a diagonal matrix element different from zero $\mathcal{D}_{nn} \neq 0$, one should consider the dipole basis states composed by dipole states oriented along $\sim \cos\phi s_x + \sin\phi s_z$, with a certain angle ϕ given by $\mathcal{D}_{nn}$. Including these corrections makes the analytical formula in general quite complicated, having a simple expression only for the ground state, which is

$$\omega_{0,0}^R = -\frac{\sqrt{\epsilon^2 + \omega_d^2 e^{-g^2/\omega_c^2}}}{2}. \quad (18)$$

However, in the USC regime $\phi \sim 0$ is a small angle and we can thus neglect it, proceeding with the simple s_x picture developed above.

In Fig. 5 we compare the real spectrum to the one obtained from the gRWA at each resonant point. In the USC limit, when $g/\omega_c \gg 1$ the agreement is very good.

The eigenstates are now given in terms of a multiphoton version of the s_x-polarized Jaynes-Cummings dressed states, fully characterized by the Hopfield coefficients $\cos\theta_{(k,n)}/2, \sin\theta_{(k,n)}/2$, generalizing the symmetric case in Appendix F. When the resonance condition $\epsilon = \omega_c \times k$ is
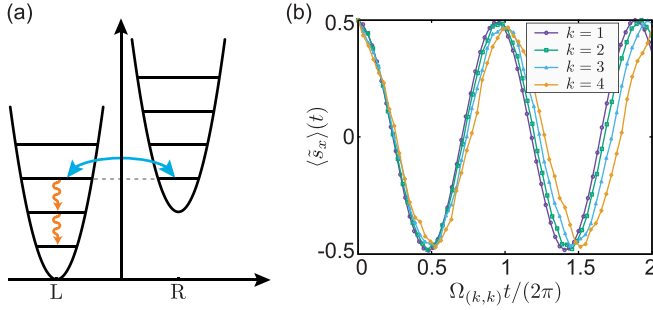
(a)

(b)

FIG. 6. (a) Schematic view of the resonant tunnel mechanism. In the USC regime, the dipole can switch well by exchanging k photons with the cavity. (b) Rabi oscillation data collapse. Each curve is labeled by its resonant index k and represents $\langle \tilde{s}_x \rangle = e^{k\gamma/2t}(\langle s_x \rangle + 1/2) - 1/2$. For each k curve the time is normalized on its respective k-Rabi frequency, $\Omega_{(k,k)}/(2\pi)$. In this way it is clear how our analytical description fits very well the full numerics. Parameters: $\omega_d = \omega_c$, $g/\omega_c = 3$, $\gamma = \kappa/4 = 0.002\omega_c$.

satisfied, the system eigenstates become

$$
\begin{aligned}
|+_{(k,n)}\rangle &= \frac{1}{\sqrt{2}}(|\leftarrow, n\rangle + |\rightarrow, n - k\rangle), \\
|-_{(k,n)}\rangle &= \frac{1}{\sqrt{2}}(|\leftarrow, n\rangle - |\rightarrow, n - k\rangle),
\end{aligned}
\tag{19}
$$

and the ground state is $|\text{GS}\rangle = |\leftarrow, 0\rangle$.

Repeating the analysis on the matrix elements in Appendix G, we realize that the s_x operator can connect only dressed states of the same (k, n) block, for which the only nondiagonal nonzero matrix element is

$$
\langle +_{(k,n)}|s_x|-_{(k,n)}\rangle = \cos \frac{\theta_{(k,n)}}{2} \sin \frac{\theta_{(k,n)}}{2}.
\tag{20}
$$

Each block is disconnected by the others, and the ground state is disconnected from all other states. Therefore relaxation toward equilibrium is still suppressed from the USC also when $\epsilon \neq 0$.

On other hand, the cavity is still able to efficiently dissipate. So, when hitting a k resonance, the dipole also can lose energy by exchanging k photons with the cavity, which are consequently flushed out. This resonant tunneling effect provides a relaxation channel for the dipole, as depicted in Fig. 6(a), and gives the proper explanation for the gaps between the lobes observed in Fig. 2(a).

We conclude this subsection by highlighting that, in the polaron frame, the USC open dynamics is mainly given by a polaronic version of the standard textbook dressed state master equation dynamics [56].

B. Multiphoton oscillations and cavity-mediated relaxation

Here we illustrate how the polaronic dressed state picture emerges clearly in the full time-dependent dynamics. As a striking example we show that the system undergoes damped Rabi oscillations, as in traditional cavity QED systems described by the Jaynes-Cummings model. However, here, depending on the resonance condition, the Rabi oscillations involve multiple photons [58–60] and must be interpreted as tunneling oscillations for the dipole.

From the block Hamiltonian in Eq. (15) we can derive the Rabi frequency of the k-resonance multiphoton Rabi oscillations reading

$$
\Omega_{(k,n)} = \omega_d \frac{g^k}{\omega_c^k} e^{-\frac{g^2}{2\omega_c^2}} L_{n-k}^{(k)}\big(g^2/\omega_c^2\big) \sqrt{\frac{(n-k)!}{n!}},
\tag{21}
$$

where $n \geqslant k$ is the total number of photons involved.

Differently from usual Rabi oscillations in cavity QED, here the dipole oscillates between the right and left states of its asymmetric double-well potential, for which we can call them *tunneling oscillations*. The relevant quantity to follow is then $\langle s_x \rangle (t)$ [as opposed to traditional Rabi oscillations, visible looking at $\langle s_z \rangle (t)$, in standard notation].

We then numerically simulate $\langle s_x \rangle (t)$ starting from the initial state $|\psi_0\rangle = |\rightarrow, 0\rangle$ (in the polaron frame). When $\gamma < \Omega_{(k,k)}$, we observe a very good fit on the curve,

$$
\langle s_x \rangle (t) \approx e^{-\frac{k\gamma}{2}t} \frac{\cos(\Omega_{(k,k)}t) + 1}{2} - \frac{1}{2}.
\tag{22}
$$

Notice that the overall decay rate is given by $\sim k \times \gamma/2$, with a factor k. This takes into account that the photon decay increases linearly with the number of photons involved, which in this case is properly k. In Fig. 6(b) we show the Rabi oscillations data collapse for various resonant values $\epsilon = \omega_c, 2\omega_c, 3\omega_c, 4\omega_c$. For each k the curve is plotted against its normalized time $\tilde{t} = \Omega_{(k,k)}t/(2\pi)$ and is normalized to remove the exponential decay accordingly to $\langle \tilde{s}_x \rangle = e^{k\gamma/2t}(\langle s_x \rangle + 1/2) - 1/2$.

C. Response functions and higher-order processes

Here we take a quick detour from the investigation of the relaxation properties of the system, and we focus our attention more specifically on how the spectral features analyzed so far manifest themselves through standard transmission measurements.

This is particularly important because current experiments, for instance, in circuit QED, cannot easily probe the time-dependent dynamics and thus have no direct access to measuring how the light-matter coupling affects relaxation. Nevertheless, since we have seen that relaxation is in the end determined by the eigenstates of the system, measuring some specific spectral features can be an indirect indication that the system follows the physics described in the previous sections.

We start considering a weak probe current entering in the LC circuit, and we look for the transmitted current. With the help of linear response theory (see Appendix H), the current response is mainly given by the cavity structure factor

$$
\mathcal{S}_c(\omega) = \frac{\hbar Z_{\text{LC}}}{2} \sum_{n,m} \frac{e^{-\hbar\omega_n/(k_b T)}}{\mathcal{Z}} |\langle n|a - a^\dagger|m\rangle|^2 \delta(\omega - \omega_{mn}).
\tag{23}
$$

Here $\mathcal{Z} = \sum_n e^{-\hbar\omega_n/(k_b T)}$ is the thermal equilibrium partition function of the system, and Z_{LC} is the characteristic cavity impedance parameter defined in Appendix B. The system circuit impedance is then defined as

$$
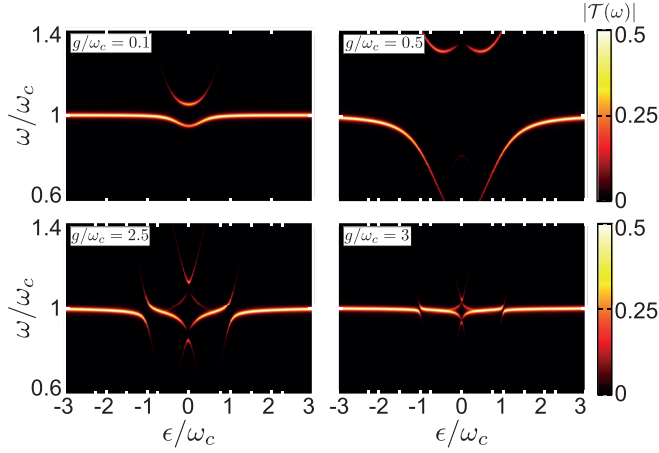Z_{\text{sys}}(\omega) = -\frac{i\omega \mathcal{S}_c(\omega)}{\hbar},
\tag{24}
$$

FIG. 7. Current transmission $|\mathcal{T}(\omega)|$ as a function of the dipole asymmetry ϵ and the probe frequency ω, for various $g/\omega_c = 0.1, 0.5, 2, 2.5$ light-matter couplings. Parameters: $\omega_d = \omega_c$, $k_bT = 0.2\hbar\omega_c$, $Q = \omega_c/\gamma = 10^2$.

and consequently the current transmission function

$$\frac{I_{\text{out}}}{I_{\text{in}}} = \mathcal{T}(\omega) = \frac{Q^{-1}}{Q^{-1} + Z_{\text{LC}}/Z_{\text{sys}}(\omega)}. \quad (25)$$

Here $Q = \omega_c/\gamma$ is the LC cavity quality factor.

In Fig. 7 we show the current transmission $|\mathcal{T}(\omega)|$ as a function of the dipole asymmetry ϵ and the probe frequency ω. To mimic experimental conditions, we consider a fixed temperature $k_bT \simeq 0.2\hbar\omega_c$.

For coupling strength up to $g/\omega_c \lesssim 0.5$ the transmission spectrum exhibits the usual Jaynes-Cummings polaritonic (or dressed state) behavior. At $\epsilon \neq 0$ the response mainly follows the bare LC circuit response, while the maximum hybridization is at $\epsilon = 0$, with maximum Rabi splitting between the upper and lower dressed state branches. This is well seen in the first panel of Fig. 7.

For increasing coupling strength, as in the second panel of Fig. 7, where $g/\omega_c = 1$, the upper branch of the transmission spectrum starts to vanish exactly at $\epsilon = 0$, signaling that we are entering the USC regime.

At even larger couplings the transmission is drastically changed. This is well seen from the two lower panels in Fig. 7, where $g/\omega_c = 2.5, 3$. In the region around $\epsilon = 0$ the transmission becomes much smaller, and the two branches related to the Jaynes-Cummings dressed states are gone. Instead the $k = 1$ avoided crossing due to the resonant tunneling is well seen around $|\epsilon|/\omega_c = 1$. The $k > 1$ higher resonances, on contrary, are not well seen, since they are covered by the bare photon resonance between the lower levels $n < k$. It is worth noticing that the ultrastrong-coupling spectral features shown here, and in particular the $k = 1$ resonance, are already visible in recent experiments with superconducting circuits [51,61–63].

Another interesting quantity to probe the spectrum of the system is provided by the dipole structure factor

$$\mathcal{S}_{\text{dip}}(\omega) = 2\hbar Z_{\text{dip}} \sum_{n,m} \frac{e^{-\hbar\omega_n/(k_bT)}}{\mathcal{Z}} |\langle n|s_x|m\rangle|^2 \delta(\omega - \omega_{mn}). \quad (26)$$
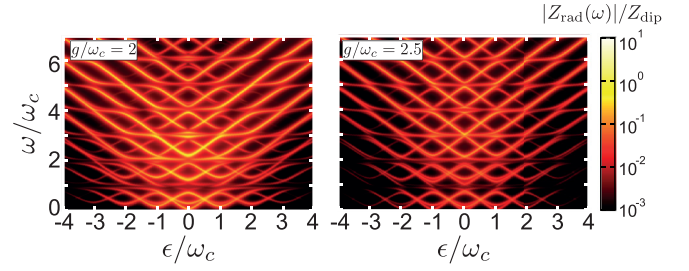

FIG. 8. Dipole radiation impedance $|Z_{\text{rad}}(\omega)|$ as a function of the dipole asymmetry ϵ and the probe frequency ω for various $g/\omega_c = 2, 2.5$ light-matter couplings. Parameters: $\omega_d = \omega_c$, $k_bT = 0.5\hbar\omega_c$. In this plot we assumed a linewidth $\gamma_{\mathcal{S}_{\text{dip}}} = 0.05\omega_c$.

The characteristic dipole impedance Z_{dip} is defined in Appendix A. From the linear response theory perspective, $\mathcal{S}_{\text{dip}}(\omega)$ quantifies the dipole radiation response to a direct drive of the dipole. Because of the consideration done in Sec. IV A, is clear that this quantity is strongly suppressed in the USC regime, at low temperature. If we stick only to the dressed state picture we should observe vanishing transitions for $T \to 0$, due to the fact that the dipole matrix element between the ground state and the first block is zero

$$\langle \pm_{(k,1)}|s_x|\text{GS}\rangle = 0. \quad (27)$$

Thus in this framework only transitions beyond the dressed state picture are visible. It is important to stress that these transitions are also present in the cavity transmission, but, since they are much weaker, they are much better visualized without the presence of the dressed state transitions which are dominant in the cavity transmission.

Similarly to the system circuit impedance we can define a dipole radiation impedance as

$$Z_{\text{rad}}(\omega) = -\frac{i\omega\mathcal{S}_{\text{dip}}(\omega)}{\hbar}. \quad (28)$$

In Fig. 8 we show the radiation impedance $Z_{\text{rad}}(\omega)$ in logscale, as a function of the dipole asymmetry ϵ and the probe frequency ω [with an artificial linewidth $\gamma_{\mathcal{S}_{\text{dip}}}$ to smear out the delta function in Eq. (26)]. Contrary to the previous case of the cavity response, at frequencies $\omega \sim \omega_c$ the dipole response is strongly suppressed in favor of higher frequencies transitions that emerge with a diamond-like pattern.

The dipole matrix elements giving the amplitude for these transitions are much weaker than the cavity-current matrix elements for the k-resonant transitions between dressed states, since are given by beyond gRWA corrections. They are the USC cavity equivalent of the vibronic transitions responsible of the Coulomb diamond structure in the Franck-Condon blockade voltage and current characteristics [37].

V. CASCADED RELAXATION IN A MULTIWELL DIPOLE

Finally we comment on the possibility to extend our results to the case of a multiwell dipole. The relaxation dynamics of this system is particularly interesting because it can be interpreted as a prototype of a transport problem through an extended system: intuitively, in a tilted multiwell potential a particle would relax from a higher well to the lowest one,

but this means that this particle is also transported from side to side in the system. Despite that a full coverage of cavity-modified relaxation or transport in an extended system is well beyond the scope of this paper, we can still use the concepts developed above to give an initial intuition which sets the basis for future investigations.

A. The extended Dicke model

We model the multiple-well dipole generalizing the two-level approximation to $(N + 1)$-level, where each level represents a potential well. In this way, the dipole is simply described by spin-$N/2$ operators, $S_{x,y,z}$ that generalize the spin description of Appendix A. In particular the eigenvalues of S_x, $|m_x\rangle$ are interpreted as localized states in the m_xth well, while the S_z operator creates some tunneling between them. This model is very similar to the well-known Wannier-Stark ladder model, where the only difference is in the nonhomogeneous hopping rates, settled by the S_z matrix element between Dicke states along the S_x direction.

While the dissipations, and the master equation, are derived in the same way as before, just replacing $s_{x,y,z} \mapsto S_{x,y,z}$ everywhere, the light-matter Hamiltonian is no longer given by the Rabi model of Eq. (1). Indeed, when taking the two-level approximation of Eq. (B5) we had discarded the x^2 term, which is only a constant within the two-level subspace, $x^2 \approx 4x_{10}^2 s_x^2 = 4x_{10}^2 \mathbb{1}$. For a multilevel dipole, described by a spin-$N/2$ system if $N > 1$ we have that $S_x^2 \neq \mathbb{1}/4$, and thus the correct cavity QED Hamiltonian within the $(N + 1)$-level subspace is given by the so-called *extended Dicke model* (EDM) [15,41]

$$H_{\text{EDM}} = \omega_c a^\dagger a + \omega_d S_z + g(a + a^\dagger)S_x + \frac{g^2}{\omega_c}S_x^2 + \epsilon S_x. \quad (29)$$

Performing the polaron transformation in the same way as for the Rabi model, we arrive at the polaron (EDM) [15]:

$$\tilde{H}_{\text{EDM}} = \omega_c a^\dagger a + \epsilon S_x + \frac{\omega_d}{2}[\mathcal{D}(g/\omega_c)\tilde{S}_+ + \mathcal{D}^\dagger(g/\omega_c)\tilde{S}_-], \quad (30)$$

where, again, $\tilde{S}_- = S_z - iS_y$. In the USC regime $g \gg \omega_c$, and for non-negligible asymmetry $\epsilon \neq 0$, in the limit of large spin, $N \gg 1$, we can use the Holstein-Primakoff approximation [64] in the S_x direction, for which $S_x \approx -N/2 + b^\dagger b$, and $\tilde{S}_- \approx \sqrt{N}b$. The polaron EDM can then be approximated by

$$\tilde{H}_{\text{EDM}} \approx \tilde{H}_{\text{EDM}}^{\text{HP}}$$

$$= \omega_c a^\dagger a + \epsilon b^\dagger b + \frac{\omega_d \sqrt{N}}{2}[\mathcal{D}(g/\omega_c)b^\dagger + \mathcal{D}^\dagger(g/\omega_c)b]. \quad (31)$$

B. Relaxation dynamics of the EDM

The considerations done for the Rabi model in Sec. IV A are still valid, in particular regarding the possibility of discarding the counter-rotating terms in the displacement operators and the suppression of tunneling. It is then clear that one can use the same dressed state approach to diagonalize the polaron EDM as well. In particular, considering the relaxation from the initial state $|0, m\rangle = (b^\dagger)^m/\sqrt{m!}|0, 0\rangle$ the resonant

tunneling effect gives rise to a cavity-mediated cascaded dynamics to the ground state, where, depending on the resonance condition $\epsilon = k \times \omega_c$, $n_{\text{ph}} \approx k \times m$ photons are released.

To have a more quantitative understanding we consider the limit of strong cavity dissipations with respect to the k-resonance splitting, $\gamma \gg \Omega_{(k,k)}$. In this regime we can adiabatically eliminate the cavity in favor of an effective master equation for the dipole only [45]. Following the previous analysis on cavity and dipole transition rates, we completely neglect the dipole dissipations, while we take as a jump operator of the cavity its bare annihilation operator $c = a$. Again, this is well motivated by the analysis performed above. Using the approximated form of the EDM in Eq. (31) and assuming that each time the total density matrix of the system is $\rho(t) \approx \rho_d(t) \otimes \rho_c^{\text{th}}$ (here ρ_c^{th} is the thermal density matrix for the bare cavity at temperature T) we have that

$$\partial_t \rho_d = -i[\epsilon b^\dagger b, \rho_d] + \frac{\Gamma_T(\epsilon)}{2}(2b\rho_d b^\dagger - [b^\dagger b, \rho_d]_+)$$

$$+ \frac{\Gamma_T(-\epsilon)}{2}(2b^\dagger \rho_d b - [bb^\dagger, \rho_d]_+). \quad (32)$$

Similarly to nonlinear optomechanics setups [65,66], the cooling and heating rates are given by

$$\Gamma_T(\omega) = \frac{\omega_d^2 N}{2}\text{Re}\left[\int_0^\infty dt(\langle \mathcal{D}(t, x)\mathcal{D}^\dagger(x)\rangle - \langle \mathcal{D}(x)\rangle^2)e^{i\omega t}\right], \quad (33)$$

where $H_c = \omega_c a^\dagger a$, $x = g/\omega_c$ and $\mathcal{D}(t, x) = e^{iH_c t}\mathcal{D}(x)e^{-iH_c t}$. Since that the average $\langle \cdot \rangle$ is intended over the cavity thermal state ρ_c^{th}, we can explicitly compute this quantity [52,65,66]

$$\Gamma_T(\omega) = \frac{\omega_d^2 N}{\gamma}e^{-x^2[1+2N_T(\omega_c)]}$$

$$\times \sum_{q,r \neq 0} \frac{x^{2r}N_T^r(\omega_c)}{r!}\frac{x^{2q}[1 + N_T(\omega_c)]^q}{q!}$$

$$\times \frac{\gamma^2/4}{[\omega - \omega_c(q - r)]^2 + \frac{\gamma^2}{4}}. \quad (34)$$

Here $N_T(\omega_c) = 1/(e^{\hbar\omega_c/(k_b T)} - 1)$ is the cavity thermal population. From this expression it is particularly evident the multiphoton character of this cavity assisted relaxation mechanism, where the dipole can relax by emitting q photons into the cavity and, at the same time, can be reexcited by absorbing r photons from the cavity (if the temperature is nonzero $T > 0$).

As in the standard theory of laser cooling the total relaxation rate is given by

$$\Gamma_T^{\text{tot}} = \Gamma_T(\epsilon) - \Gamma_T(-\epsilon). \quad (35)$$

At $T = 0$ and close to resonance $\epsilon \simeq \omega_c \times k$, the total relaxation rate is approximately given by $\Gamma_{T=0}^{\text{tot}} \approx \Omega_{(k,k)}^2 N/\gamma$, which is the USC version of the Purcell effect. In Fig. 9 we show some examples of the total relaxation rate for $T = 0$ and for $T > 0$ at different coupling strengths. Interestingly a higher temperature may help in activating the higher k resonances even in the non-USC regime, $g/\omega_c \ll 1$, resembling the behavior of optomechanical laser cooling setups [67]. We
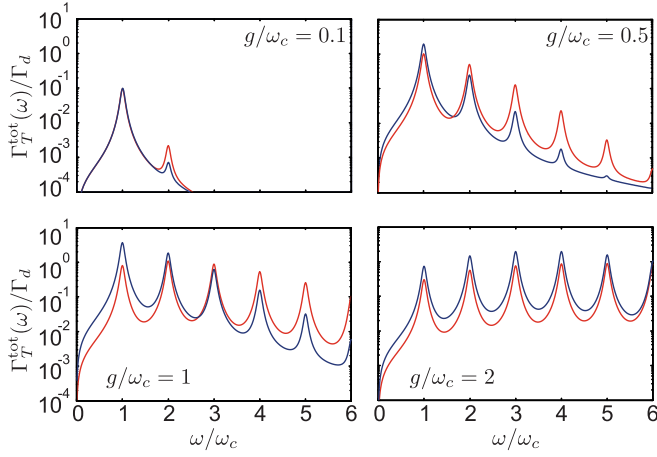
FIG. 9. Total relaxation rate $\Gamma_T^{\text{tot}}(\omega)$ defined in Eq. (35) as a function of frequency ω for various $g/\omega_c = 0.1, 0.5, 1, 2$ coupling strengths (normalized over $\Gamma_d = \omega_d^2 N/\gamma$). The blue line corresponds to $T = 0$, and the red line is for $k_b T = 2 \hbar \omega_c$. Parameters: $\gamma/\omega_c = 0.1$.

highlight the fact that at weak coupling this description does not hold, since it is based on the assumption that dipole tunneling is suppressed by the USC regime. However, we found it interesting to show the total relaxation rate Γ_T^{tot} also in this regime for completeness.

As anticipated in the beginning of this section, the relaxation dynamics of this multiwell setup can be seen as a way to study how the incoherent transport is modified by the cavity. Staying at the single-particle level we can interpreted an excitation produced by the dipole operator $b^\dagger$ as the particle moving one well up in energy, and the dipole ground state as the state where only the lowest energy well is occupied. Following this line of thought, we can say that the system has good transport properties if it rapidly thermalizes sufficiently close to its ground state. Since the saturation number of the steady state of Eq. (32), $\langle b^\dagger b \rangle_{\text{ss}} = \mathcal{N}_0$, around each k resonance $\epsilon = \omega_c \times k$ is the dipole thermal occupation

$$\mathcal{N}_0 = \frac{\Gamma_T(-\epsilon)}{\Gamma_T(\epsilon) - \Gamma_T(-\epsilon)} \approx N_T(\omega_c \times k), \qquad (36)$$

we also need that the temperature T is small enough so thermal photons cannot push the particle (the dipole excitation) to an upper energy level.

In summary, the cavity USC suppresses tunneling also in a multiwell dipole scenario, inhibiting the dipole's relaxation and its ability to transport excitations from one well to the other. Fast relaxation (and transport) is possible only when the tilted multiwell dipole is resonant with the cavity having access to the multiphoton resonant tunneling process.

VI. CONCLUSION

In conclusion, we studied the relaxation properties of a simple (but paradigmatic) cavity QED setup in the ultrastrong coupling regime described by the asymmetric quantum Rabi model. Here the bosonic cavity mode is provided by an LC resonant circuit, while the two-level atom is given by an asymmetric dipole inside the capacitor of the LC circuit. We

introduce dissipation by considering the cavity coupled to a Ohmic transmission line, while the dipole dissipates into radiating modes with super-Ohmic spectral density. The system's dynamics is thus described by a thermalizing master equation, valid at arbitrary light-matter coupling strengths and arbitrary dipole asymmetry. From the Liouvillian gap we obtained the longest relaxation rate of the system that we can also consider its asymptotic thermalization rate. From this quantity emerges clearly that the effect of the USC is to slow the system's thermalization by an exponential suppression of the Liouvillian gap. However, for special values of the dipole asymmetry the standard relaxation is restored and the system can thermalize accordingly to its bare relaxation rates.

To understand this behavior of the Liouvillian gap and to link it to the physical observables of the system, we employed a generalized rotating-wave approximation (gRWA) [55], valid in the so-called polaron frame. Within this approximation we showed that is possible to analytically diagonalize the asymmetric Rabi model, even in the USC regime, where the eigenstates are given by a polaronic multiphoton version of the usual Jaynes-Cummings dressed states. In this way we were able to compute the relaxation rates in the USC regime analytically, explicitly showing the exponential slow-down of thermalization due to an effective suppression of the dipole tunneling dynamics, while the cavity, remaining effectively uncoupled from the dipole, can still efficiently relax.

When the dipole asymmetry is resonant with the cavity, the dipole dynamics is revitalized, by a cavity-assisted tunneling, where the dipole resonantly tunnels from one well to the other by releasing multiple photons. Since photons can then relax out of the cavity, this process gives an effective relaxation channel also for the dipole.

After showing that these phenomenon can be observed indirectly from the cavity transmission or the dipole impedance, we highlight a link to the Franck-Condon physics of electronic transport through a molecular dot [9,37].

At the end, we commented on the possibility of extending this nonlinear resonant processes to a multiwell dipole. A simple toy model to describe this situation is provided by the extended Dicke model, introduced originally to study a multiple qubit ultrastrongly coupled to a single LC cavity [15,41]. From this setup it is clear that the USC resonant tunnel dynamics can affect also a multiwell system, giving rise to a resonant cascaded multiphoton process. We argue that this cascaded effect could be observed in cavity-modified transport experiments with multiple electronic quantum dots, or in superconducting circuit devices with only minor modifications of the already existing platforms [9,51]. This suggests that these findings could thus provide an interesting playground to study an implementation for cascaded-laser electronic devices operating in the USC regime in the GHz or THz range.

APPENDIX A: A DIPOLE IN A ASYMMETRIC DOUBLE WELL POTENTIAL

The dipole dynamics is described as a single particle with mass m in a potential

$$H_{\text{dipole}} = \frac{p^2}{2m} + V(x). \tag{A1}$$

The dipole has charge $+q$ on an extreme and $-q$ on the other extreme, and qx is its dipole moment. So the dipole displacement x is its main dynamical variable and p its canonical momentum.

As depicted in Fig. 1(b), we consider only the paradigmatic case of a dipole described by a double-well potential, very similarly to Refs. [68,69]. Considering only its low-energy dynamics we are basically studying the electromagnetism of quantum tunneling.

Differently from Ref. [15] here we introduce a linear tilt that makes the height of the two wells asymmetric. The total dipole's potential is then given by

$$V(x) = -\frac{\mu_2^2}{2} x^2 + \frac{\mu_4^4}{4} x^4 + q\mathcal{E}x. \tag{A2}$$

The linear tilt $\sim q\mathcal{E}x$ is physically implemented by a bias static external electric field of amplitude $\mathcal{E}$ and has no influence on the LC resonator dynamics.

Whenever $\mu_2/\mu_4 \gg 1$ and $q\mathcal{E}/\mu_2 \ll 1$, the two lowest levels are below the central barrier and well separated from the other energy levels. We can then truncate the dipole's Hilbert space keeping only these two lowest energy levels [15]. We perform the two-level approximation (TLA) on the dipole Hamiltonian projecting on the eigenstates without tilt $\mathcal{E} = 0$, and we obtain

$$H_{\text{dipole}}^{\text{TLA}} = \hbar\omega_d s_z + \hbar\epsilon s_x. \tag{A3}$$

Here we have introduced the pseudospin operators $s_a = \sigma_a/2$ (σ_a are the usual Pauli matrices). The dipole frequency ω_d is the energy difference between the two lowest states without the tilt $\mathcal{E} = 0$, and $\epsilon = 2q\mathcal{E}x_{10}/\hbar$, where $x_{10} = \langle 1|x|0\rangle$ is the dipole matrix element between the two lowest dipole states. The dipole operator now is given by $x \approx x_{10}\sigma_x$.

When the tilt is on, the energy splitting between the two eigenstates of Eq. (A3) is given by $\omega_\epsilon = \sqrt{\omega_d^2 + \epsilon^2}$, while the eigenfunctions are partially localized on the left or right well, with a small, but non-negligible, overlap with the opposite well [Fig. 1(b)]. In the two-level language these states are given by

$$\begin{aligned} |\text{L}_\epsilon\rangle &= \cos\frac{\theta_\epsilon}{2}|\downarrow\rangle + \sin\frac{\theta_\epsilon}{2}|\uparrow\rangle, \\ |\text{R}_\epsilon\rangle &= -\sin\frac{\theta_\epsilon}{2}|\downarrow\rangle + \cos\frac{\theta_\epsilon}{2}|\uparrow\rangle, \end{aligned} \tag{A4}$$

where $\tan(\theta_\epsilon) = \epsilon/\omega_d$.

We can also associate a characteristic impedance with the dipole by considering $Z_{\text{dip}} = \hbar/q^2 f_{10}$, and $f_{10} = 2m\omega_0|x_{10}|^2/\hbar$ is the oscillator strength of the two-level dipole transition. Introducing this parameter is particularly convenient when discussing the linear response theory and creates a nice parallelism with the circuit description of the cavity given in what follows.

APPENDIX B: GENERAL CAVITY QED HAMILTONIAN

The Hamiltonian of the full cavity QED system can be written summing up the dipole energy and the total energy stored in the electromagnetic field

$$H_{\text{cQED}} = H_{\text{em}} + H_{\text{dipole}}. \tag{B1}$$

For an LC-resonant system, the electromagnetic energy is described by

$$H_{\text{em}} = \frac{CU^2}{2} + \frac{\Phi^2}{2L}, \tag{B2}$$

where U is the total voltage drop across the capacitor C, and Φ is the magnetic flux through the inductance L.

When the dipole is inside the capacitor the total voltage U is no longer the right canonical variable conjugate to Φ. In order to have the correct canonical description we need to introduce the total capacitor charge variable Q, such that $[\Phi, Q] = i\hbar$. Without the presence of the dipole the total charge and the voltage drop are directly proportional through the usual relation $U = CQ$. When the dipole is inside the capacitor the charge responsible for the voltage drop is modified by the presence of the charge induced by the dipole on the metallic plates. This induced charge does not contribute to any voltage drop and must be removed [15,41]. The voltage drop becomes

$$U = C(Q - Q_{\text{ind}}). \tag{B3}$$

For an ideal capacitor we have $Q_{\text{ind}} \simeq qx/d$ [15], where d is the distance between the capacitor plates.

We introduce now the cavity creation and annihilation operators through the relations

$$\begin{aligned} \Phi &= i\frac{\Phi_0}{\sqrt{2}}(a - a^\dagger), \\ Q &= \frac{Q_0}{\sqrt{2}}(a + a^\dagger). \end{aligned} \tag{B4}$$

Here $\Phi_0 = \sqrt{\hbar Z_{\text{LC}}}$, $Q_0 = \sqrt{\hbar/Z_{\text{LC}}}$, and $Z_{\text{LC}} = \sqrt{L/C}$. The cavity QED reads

$$H_{\text{cQED}} = \hbar\omega_c a^\dagger a + H_{\text{dipole}} + F_0 x(a + a^\dagger) + \frac{F_0^2}{\hbar\omega_c}x^2, \tag{B5}$$

where $\omega_c = 1/\sqrt{LC}$ and we introduced the zero-point electric force $F_0 = \sqrt{\hbar\omega_c/(2Cd^2)q^2}$.

As detailed in Refs. [68,69], implementing the TLA described in Appendix A, we can now approximate the cavity QED Hamiltonian with the so-called *quantum Rabi model* ($\hbar = 1$)

$$H_{\text{cQED}} \approx H_{\text{Rabi}} = \omega_c a^\dagger a + \omega_d s_z + \epsilon s_x + g(a + a^\dagger)s_x, \tag{B6}$$

where the light-matter coupling is given by $g = 2F_0 x_{10}$.

We will see in particular that the transverse term $\sim\epsilon s_x$, which breaks the $\mathbb{Z}_2$ symmetry of the usual Rabi model, is fundamental in our development, becoming a switch between slow and fast dissipation of the dipole. In circuit QED this term emerges quite naturally through a bias in the external magnetic flux and is typically used in the observation of the spectral features of the USC regime [51,62].

APPENDIX C: LINEAR DAMPING

This Appendix reviews the standard derivation of the Langevin equation for open quantum systems as is developed in standard textbooks [45,70], which sets the basis for the formalism that we use through the whole paper.

We consider a generic system, described by the Hamiltonian H_{sys}, coupled to a bath of harmonic oscillators (which may represent the electromagnetic field outside of a cavity, or a resistance in a circuit):

$$H = H_{\text{sys}} + \sum_k \left[\frac{P_k^2}{2m_k} + \frac{1}{2} m_k \omega_k^2 \left(Y_k - \frac{c_k}{m_k \omega_k^2} X \right)^2 \right]. \quad \text{(C1)}$$

The equations of motion for a generic system operator A are given by

$$\partial_t A = -i[A, H_{\text{sys}}] + i \sum_k \frac{c_k}{2} (Y_k[A, X] + [A, X]Y_k)$$

$$- i \sum_k \frac{c_k^2}{2m_k \omega_k^2} [A, X^2], \quad \text{(C2)}$$

$$\partial_t Y_k = \frac{P_k}{m_k}, \quad \partial_t P_k = -m_k \omega_k^2 Y_k + c_k X. \quad \text{(C3)}$$

The formal solution of the bath's equations is given by

$$Y_k(t) = Y_k^{\text{homg.}}(t) + \frac{c_k}{m_k \omega_k} \int_{t_0}^t dt' \sin[\omega_k(t - t')] X(t'), \quad \text{(C4)}$$

where

$$Y_k^{\text{homg.}}(t) = Y_k(t_0) \cos[\omega_k(t - t_0)] + \frac{P_k(t_0)}{m_k \omega_k} \sin[\omega_k(t - t_0)]. \quad \text{(C5)}$$

Plugging back this solution into (C2), and integrating by part, we get the quantum Langevin equation, describing the whole open-dissipative dynamics of our quantum system

$$\partial_t A(t) = -i[A(t), H_{\text{sys}}]$$

$$+ \frac{i}{2} \{ \xi(t)[A(t), X(t)] + [A(t), X(t)] \xi(t) \}$$

$$- \frac{i}{2} \left[\int_{t_0}^t K(t - t') \partial_{t'} X(t') \, dt', \, [A(t), X(t)] \right]_+. \quad \text{(C6)}$$

Here $[\cdot, \cdot]_+$ is the anticommutator, and

$$\xi(t) = \sum_k c_k \left(Y_k^{\text{homg.}}(t) - \frac{c_k}{m_k \omega_k^2} X(t_0) \cos[\omega_k(t - t_0)] \right)$$

$$K(t) = \sum_k \frac{c_k^2}{m_k \omega_k^2} \cos(\omega_k t) \quad \text{(C7)}$$

are, respectively, the *quantum noise term* and the *dissipative kernel*. We notice that the last term in (C2) is exactly canceled by the term proportional to $K(t)$ coming out by the integration by part. From the fluctuation-dissipation theorem we obtain the specific value of the quantum noise correlator [70]. In the high-temperature limit it reads

$$\frac{1}{2} \langle [\xi(t), \xi(t')]_+ \rangle \simeq 2k_b T K(t - t'). \quad \text{(C8)}$$

The in and out relations are given by [70]

$$Y^{\text{out}}(t) = Y^{\text{in}}(t) - \int_{-\infty}^{+\infty} K(t - t') \dot{X}(t') \, dt', \quad \text{(C9)}$$

where $Y^{\text{in}}(t) = \sum_k c_k Y_k^{\text{homg.}}(t)$.

A useful way to treat the dissipation without having all the details of the bath is to introduce the bath spectral density

$$J(\omega) = \frac{\pi}{2} \sum_k \frac{c_k^2}{m_k \omega_k} \delta(\omega - \omega_k), \quad \text{(C10)}$$

and recast the dissipator in the form

$$K(t) = \int_0^\infty \frac{d\omega}{\pi} \frac{J(\omega)}{\omega} \cos(\omega t). \quad \text{(C11)}$$

Now all bath properties are encoded in the spectral density $J(\omega)$.

APPENDIX D: THERMALIZING MASTER EQUATION

We consider here the master equation suitable for studying relaxation and thermalization processes in cavity QED under the ultrastrong coupling regime. For this purpose we consider the treatment used in [54]. We do not repeat the derivation here, but we stress that the physical assumptions are almost the same as used in deriving the Langevin equation in Appendix C, with the further assumption that the coupling between the system and the bath is very small. In particular this latter one ensures that we can implement the rotating wave approximation between the system and the bath, proceeding with the standard textbook derivation.

The crucial step here is to isolate the components of the system coupling operator X that rotates with positive (negative) frequencies. This can be done as follows: given an Hamiltonian H_{sys} and a (or multiple) system operator(s) X, we express them on the system eigenbasis $X = \sum_{n,m} \langle n|X|m \rangle |n\rangle\langle m|$. The jump operators are then given by the set $\{ c_{nm} = \langle n|X|m \rangle |n\rangle\langle m|, \text{ such that } n < m \}$. In the Heisenberg picture these jump operators evolve with positive frequencies. This allows us to implement the rotating wave approximation in the standard system-bath linear Hamiltonian in Eq. (C1).

The master equation is then given by

$$\partial_t \rho = \mathcal{L}_H(\rho) + \mathcal{L}_D(\rho), \quad \text{(D1)}$$

where the conservative time evolution is generated by

$$\mathcal{L}_H(\rho) = -i[H_{\text{sys}}, \rho], \quad \text{(D2)}$$

while dissipations are given by

$$\mathcal{L}_D(\rho) = \sum_{n<m} [1 + N_T(\omega_{mn})] \Gamma_{nm} D(|n\rangle\langle m|, \rho)$$

$$+ \sum_{n<m} N_T(\omega_{mn}) \Gamma_{nm} D(|m\rangle\langle n|, \rho). \quad \text{(D3)}$$

Here

$$D(c, \rho) = c \, \rho \, c^\dagger - \frac{1}{2} [c^\dagger c, \, \rho]_+ \quad \text{(D4)}$$

is the usual dissipator super-operator [45], and

$$N_T(\omega) = \frac{1}{e^{\omega/(k_B T)} - 1} \quad \text{(D5)}$$

is the bosonic thermal population, where k_B is the Boltzmann constant. The thermalization rates are given by

$$\Gamma_{nm} = J(|\omega_{mn}|)|\langle n|X|m\rangle|^2. \tag{D6}$$

It is important to keep in mind here that there is another implicit assumption to correctly use this master equation: the energy levels are well resolved with respect to the bath-induced linewidth, meaning that $\Gamma_{nm} \ll \omega_{nm}$. Considering only weak losses and not too weak nor not too strong coupling, we can consider it always satisfied in our development.

Considering the thermal density matrix $\rho_{\rm ss} = e^{-H_{\rm sys}/(k_B T)}/\mathcal{Z}$, where $\mathcal{Z} = {\rm Tr}[\rho_{\rm ss}]$, one can easily prove that is the steady state of the system.

APPENDIX E: PHYSICAL DISSIPATORS

1. Cavity dissipation

A standard way to introduce dissipation in an LC circuit is to couple it to a transmission line [45]. When it is traced out from the dynamics, the transmission line plays the role of a resistive element, effectively realizing the scheme described in Fig. 1(c). An input voltage can inject current in the system, and the resistance dampens the excited oscillations of the LC circuit. This scheme provides a basic input and output theory describing the system's readout from the energy dissipated into the resistance.

The formal description of this setup assumes a linear coupling to a multimode bath of harmonic modes, as shown in Eq. (C1) of Appendix C. To realize the resistive circuit, since $\Phi = LI$ is linked to the current passing through the inductor (and so through the whole circuit) the system operator coupled to the bath is [45,52,71]

$$\hat{X} = \Phi = i\frac{\Phi_0}{\sqrt{2}}(a - a^\dagger). \tag{E1}$$

To reproduce a standard Ohmic resistance we assume the standard linear spectral density (neglecting for now the correct dimensional units)

$$J_{\rm Ohm}(\omega) \sim \gamma\omega. \tag{E2}$$

Eliminating the bath's dynamics, we obtain the equations of motion of the circuit in terms of the Langevin equation in Eq. (C6), and, considering $A = \dot{\Phi}$ in Eq. (C6), we have that

$$\ddot{\Phi} \sim -\gamma\dot{\Phi}, \tag{E3}$$

correctly matching the standard Kirchhoff equations of a resistive circuit.

To implement the thermalizing master equation used in the main text, we introduce the jump operators corresponding to this decay channel as

$$c_{nm}^c = \langle n|a - a^\dagger|m\rangle |n\rangle\langle m|, \tag{E4}$$

where $m > n$ and $|n\rangle$ are the eigenstates of the whole system, in such a way that they correctly describe the relaxation process from higher to lower energy states, even when the system is ultrastrongly coupled; see Appendix D.

Since in our theory the coefficient γ is a free parameter, we absorb the dimensional quantity $\Phi_0/\sqrt{2}$ in the definition

of the spectral density, such that

$$\frac{\omega_c|\Phi_0|^2}{2}J_{\rm Ohm}(\omega) \longmapsto J_{\rm Ohm}(\omega). \tag{E5}$$

2. Dipole dissipation

In our simplified picture, the main source of dissipation of an oscillating electric dipole is given by radiative emission into free space electromagnetic modes. Indeed, even if the dipole is strongly coupled to the subwavelength mode of the LC cavity, it still interacts with all the other transverse electromagnetic modes. These have typically a small effect on the coherent dynamics [36], but they provide a decay channel for the dipole.

Because of the harmonic dynamics of the electromagnetic field, and its general linear coupling with the dipole, we can again model the dipole dissipation as a linear damping, as described in Appendix C. In this case the system operator coupled to the dissipative bath is given by the dipole moment

$$\hat{X} = x \approx 2x_{10}s_x. \tag{E6}$$

The bath spectral function is given from the spectral function of the transverse electromagnetic modes. In free space this would be given approximately by (neglecting the dimensionality, the correct dimensional units will be reintroduced in the next section)

$$J_{\rm rad}(\omega) \sim \kappa\omega^3. \tag{E7}$$

Considering the Langevin equation in Eq. (C6) for the dipole moment velocity $A = \dot{x}$, using this spectral density we find

$$\dddot{x} \sim \kappa\dddot{x}, \tag{E8}$$

recovering the Abraham-Lorentz formula for a radiating dipole [72].

More generally for our developments, one can choose any spectral density for the dipole dissipative bath of the shape $J_{\rm rad} \sim \omega^\nu$, with $\nu \geqslant 1$. Having $\nu > 1$ gives particularly simple results.

As for the cavity, the jump operators corresponding to this decay channel are

$$c_{nm}^{\rm dip} = \langle n|s_x|m\rangle |n\rangle\langle m|, \tag{E9}$$

where $m > n$ and $|n\rangle$ are the eigenstates of the whole system, in such a way that they correctly describe the relaxation process from higher to lower energy states, even when the system is ultrastrongly coupled; see Appendix D.

Since also here κ is a free parameter, we absorb the dimensional quantity $2x_{10}$ in the definition of the spectral density, such that

$$4\omega_d|x_{10}|^2 J_{\rm rad}(\omega) \longmapsto J_{\rm rad}(\omega). \tag{E10}$$

APPENDIX F: DIAGONALIZATION OF THE RESONANT-SYMMETRIC RABI HAMILTONIAN

In this section we perform the approximated diagonalization of the Rabi model in the regime where

$$\omega_d \simeq \omega_c,$$
$$\epsilon = 0. \tag{F1}$$

We first transform the original Rabi Hamiltonian through the unitary transformation $U_{\text{pol}} = \exp[g/\omega_c(a - a^\dagger)s_x]$, obtaining the Rabi polaron Hamiltonian in the form

$$\tilde{H}_{\text{Rabi}} = \omega_c a^\dagger a + \omega_d\{\cosh[g/\omega_c(a - a^\dagger)]s_z$$
$$+ i\sinh[g/\omega_c(a - a^\dagger)]s_y\}. \quad \text{(F2)}$$

Here cosh and sinh operators can be expressed in terms of the displacement operator $\mathcal{D}(x) = \exp[x(a - a^\dagger)]$.

In this frame one can then perform a generalized rotating wave approximation [55], following from the fact that the Hamiltonian in this basis is approximately block diagonal. Each block is spanned by the states $\{|\uparrow, n - 1\rangle, |\downarrow, n\rangle\}$, where $n = 1, 2\ldots$, and the ground state is given by the polaron vacuum state $|\downarrow, 0\rangle$.

This block-diagonal structure is ultimately linked to the matrix elements of the displacements operators in Eq. (F2), which are known to be exponentially suppressed as $\langle n|\mathcal{D}(g/\omega_c)|m\rangle \sim e^{-g^2/(2\omega_c^2)}$ [57]. Moreover because of parity selection rule of the $\cosh[g/\omega_c(a - a^\dagger)]s_z$, $\sinh[g/\omega_c(a - a^\dagger)]s_y$ operators that are only second nearest-neighbor blocks are coupled. Combining these two observations we have that the most relevant transitions are within each block, for which we need only two matrix elements of the displacement operator per block:

$$\mathcal{D}_{n\,n-1} = \frac{g}{\omega_c}\sqrt{\frac{(n-1)!}{n!}}e^{-\frac{g^2}{2\omega_c^2}}L_{n-1}^{(1)}(g^2/\omega_c^2),$$
$$\mathcal{D}_{nn} = e^{-\frac{g^2}{2\omega_c^2}}L_n^{(0)}(g^2/\omega_c^2), \quad \text{(F3)}$$

where $L_n^{(\alpha)}(x)$ are the special Laguerre polynomials. Notice that, since $L_n^{(\alpha)}(0) = (n + \alpha)!/(n!)$, we have that $L_{n-1}^{(1)}(0) = n$, recovering the usual Jaynes-Cummings picture at weak coupling.

We can then rewrite the polaron Rabi Hamiltonian as a block-diagonal matrix, $\tilde{H}_{\text{Rabi}} \approx \sum_n \tilde{H}_{\text{Rabi}}^n$, where each block reads

$$\tilde{H}_{\text{Rabi}}^n = \begin{pmatrix} A_n & C_n \\ C_n & B_n \end{pmatrix}, \quad \text{(F4)}$$

where

$$A_n = \omega_c n - \frac{\omega_d e^{-g^2/(2\omega_c^2)}}{2}L_n^{(0)}(g^2/\omega_c^2),$$
$$B_n = \omega_c(n - 1) + \frac{\omega_d e^{-g^2/(2\omega_c^2)}}{2}L_{n-1}^{(0)}(g^2/\omega_c^2),$$
$$C_n = \frac{g}{\omega_c}\frac{\omega_d e^{-g^2/(2\omega_c^2)}}{2}\sqrt{\frac{(n-1)!}{n!}}L_{n-1}^{(1)}(g^2/\omega_c^2). \quad \text{(F5)}$$

The spectrum is

$$\omega_{\pm,n} = \frac{A_n + B_n}{2} \pm \sqrt{\frac{(A_n + B_n)^2}{4} + C_n^2 - A_n B_n}, \quad \text{(F6)}$$

and the eigenstates are

$$|+, n\rangle = \cos\frac{\theta_n}{2}|\downarrow, n\rangle + \sin\frac{\theta_n}{2}|\uparrow, n - 1\rangle,$$
$$|-, n\rangle = -\sin\frac{\theta_n}{2}|\downarrow, n\rangle + \cos\frac{\theta_n}{2}|\uparrow, n - 1\rangle, \quad \text{(F7)}$$

where

$$\cos\frac{\theta_n}{2} = \pm\sqrt{\frac{1}{2}\left(1 + \frac{A_n - B_n}{\sqrt{(A_n - B_n)^2 + 4C_n^2}}\right)},$$
$$\sin\frac{\theta_n}{2} = \pm\sqrt{\frac{1}{2}\left(1 - \frac{A_n - B_n}{\sqrt{(A_n - B_n)^2 + 4C_n^2}}\right)}. \quad \text{(F8)}$$

This approximate solution of the symmetric Rabi model is valid in all coupling regimes for each value of g. However, its validity is restricted to the cases when $\omega_d \lesssim \omega_c$ [55].

APPENDIX G: MATRIX ELEMENT AND TRANSITION RATES OF THE SYMMETRIC RABI MODEL

As for standard dressed states, the allowed transitions are only between states of neighboring blocks, with $(n, n \pm 1)$-excitations, and the only relevant matrix elements contributing to the transition rates of the cavity are

$$\langle +, n|(a^\dagger - a)|-, n - 1\rangle$$
$$= \sqrt{n - 1}\cos\frac{\theta_{n-1}}{2}\sin\frac{\theta_n}{2} - \sqrt{n}\cos\frac{\theta_n}{2}\sin\frac{\theta_{n-1}}{2}, \quad \text{(G1)}$$

$$\langle -, n|(a^\dagger - a)|+, n - 1\rangle$$
$$= \sqrt{n - 1}\sin\frac{\theta_{n-1}}{2}\cos\frac{\theta_n}{2} - \sqrt{n}\sin\frac{\theta_n}{2}\cos\frac{\theta_{n-1}}{2}, \quad \text{(G2)}$$

$$\langle +, n|(a^\dagger - a)|+, n - 1\rangle$$
$$= \sqrt{n - 1}\sin\frac{\theta_{n-1}}{2}\sin\frac{\theta_n}{2} + \sqrt{n}\cos\frac{\theta_n}{2}\cos\frac{\theta_{n-1}}{2}, \quad \text{(G3)}$$

$$\langle -, n|(a^\dagger - a)|-, n - 1\rangle$$
$$= \sqrt{n - 1}\cos\frac{\theta_{n-1}}{2}\cos\frac{\theta_n}{2} + \sqrt{n}\sin\frac{\theta_n}{2}\sin\frac{\theta_{n-1}}{2}, \quad \text{(G4)}$$

and for the ground state

$$\langle \downarrow, 0|(a^\dagger - a)|+, 1\rangle = -\cos\frac{\theta_1}{2},$$
$$\langle \downarrow, 0|(a^\dagger - a)|-, 1\rangle = \sin\frac{\theta_1}{2}. \quad \text{(G5)}$$

For the dipole we have a complementary situation

$$\langle +, n|s_x|-, n - 1\rangle = -\frac{1}{2}\sin\frac{\theta_{n-1}}{2}\sin\frac{\theta_n}{2}, \quad \text{(G6)}$$

$$\langle -, n|s_x|+, n - 1\rangle = \frac{1}{2}\cos\frac{\theta_{n-1}}{2}\cos\frac{\theta_n}{2}, \quad \text{(G7)}$$

$$\langle +, n|s_x|+, n - 1\rangle = \frac{1}{2}\cos\frac{\theta_{n-1}}{2}\sin\frac{\theta_n}{2}, \quad \text{(G8)}$$

$$\langle -, n|s_x|-, n - 1\rangle = -\frac{1}{2}\sin\frac{\theta_{n-1}}{2}\cos\frac{\theta_n}{2}, \quad \text{(G9)}$$

and the ground state

$$\langle\downarrow, 0|s_x|+, 1\rangle = \sin\frac{\theta_1}{2},$$

$$\langle\downarrow, 0|s_x|-, 1\rangle = \cos\frac{\theta_1}{2}. \tag{G10}$$

APPENDIX H: LINEAR RESPONSE AND ABSORPTION SPECTRA

Exciting the cavity corresponds to inserting a current in the circuit, which can be interpreted as a parallel LC filter. We can then define a system circuit impedance $Z_{\text{sys}}(\omega)$ for the LC circuit, which takes into account the presence of the dipole in the capacitor. By using the standard composition of circuit impedance, we can derive the response input and output relations from the current flowing in the resistance (the transmission line)

$$\frac{I_{\text{out}}}{I_{\text{in}}} = \frac{Z_{\text{sys}}(\omega)}{R + Z_{\text{sys}}(\omega)}, \tag{H1}$$

where $R = Z_{\text{LC}}Q$ is the Ohmic resistance of the transmission line coupled to the LC cavity, and $Q = \omega_c/\gamma$ is the LC cavity quality factor. In Fig. 1(c) it is shown the general scheme of our circuit approach.

The system impedance is defined by considering the relation between voltage and current flowing through the circuit, $V = ZI$, which gives

$$Z_{\text{sys}}(\omega) = \frac{\langle\dot{\Phi}\rangle(\omega)}{I_{\text{in}}(\omega)}. \tag{H2}$$

When the input current is very small we can invoke linear response theory [73], for which we have

$$\chi_{VI} = \lim_{I_{\text{in}}\to 0} \frac{\langle\dot{\Phi}\rangle(\omega)}{I_{\text{in}}(\omega)}, \tag{H3}$$

where χ_{VI} is the voltage-current linear response function [73]. From here it follows an operative definition of the system impedance as

$$Z_{\text{sys}}(\omega) = -i\omega\chi_{II}(\omega), \tag{H4}$$

where

$$\chi_{II} = \lim_{I_{\text{in}}\to 0} \frac{\langle\Phi\rangle(\omega)}{I_{\text{in}}(\omega)} \tag{H5}$$

is the current-current linear response function.

The current-current linear response function can be calculated in many ways, but the simplest one is to use the cavity structure factor

$$\mathcal{S}_c(\omega) = \sum_{n,m} \frac{e^{-\hbar\omega_n/(k_b T)}}{\mathcal{Z}} |\langle n|\Phi|m\rangle|^2 \delta(\omega - \omega_{mn}). \tag{H6}$$

The system impedance is then given by $Z_{\text{sys}}(\omega) = -i\omega\mathcal{S}_c(\omega)$.

---

[1] L. Landau and E. Lifshitz, *Statistical Physics*, Vol. 5 (Elsevier Science, Amsterdam, 2013).

[2] Z. A. Piskulich, O. O. Mesele, and W. H. Thompson, Activation energies and beyond, J. Phys. Chem. A **123**, 7185 (2019).

[3] E. Merzbacher, The early history of quantum tunneling, Phys. Today **55**, 44 (2002).

[4] A. O. Caldeira and A. J. Leggett, Influence of dissipation on quantum tunneling in macroscopic systems, Phys. Rev. Lett. **46**, 211 (1981).

[5] A. J. Leggett, S. Chakravarty, A. T. Dorsey, M. P. A. Fisher, A. Garg, and W. Zwerger, Dynamics of the dissipative two-state system, Rev. Mod. Phys. **59**, 1 (1987).

[6] P. Milonni, *The Quantum Vacuum: An Introduction to Quantum Electrodynamics* (Elsevier Science, Amsterdam, 1994).

[7] J. A. Hutchison, T. Schwartz, C. Genet, E. Devaux, and T. W. Ebbesen, Modifying chemical landscapes by coupling to vacuum fields, Angew. Chem., Int. Ed. **51**, 1592 (2012).

[8] G. L. Paravicini-Bagliani, F. Appugliese, E. Richter, F. Valmorra, J. Keller, M. Beck, N. Bartolo, C. Rössler, T. Ihn, K. Ensslin *et al.*, Magneto-transport controlled by Landau polariton states, Nat. Phys. **15**, 186 (2019).

[9] F. Valmorra, K. Yoshida, L. C. Contamin, S. Messelot, S. Massabeau, M. R. Delbecq, M. C. Dartiailh, M. M. Desjardins, T. Cubaynes, Z. Leghtas *et al.*, Vacuum-field-induced THz transport gap in a carbon nanotube quantum dot, Nat. Commun. **12**, 5490 (2021).

[10] F. Appugliese, J. Enkner, G. L. Paravicini-Bagliani, M. Beck, C. Reichl, W. Wegscheider, G. Scalari, C. Ciuti, and J. Faist, Breakdown of topological protection by cavity vacuum fields in the integer quantum Hall effect, Science **375**, 1030 (2022).

[11] J. Flick, M. Ruggenthaler, H. Appel, and A. Rubio, Atoms and molecules in cavities, from weak to strong coupling in quantum-electrodynamics (QED) chemistry, Proc. Natl. Acad. Sci. USA **114**, 3026 (2017).

[12] J. Fregoni, F. J. Garcia-Vidal, and J. Feist, Theoretical challenges in polaritonic chemistry, ACS Photonics **9**, 1096 (2022).

[13] C. Schäfer, J. Flick, E. Ronca, P. Narang, and A. Rubio, Shining light on the microscopic resonant mechanism responsible for cavity-mediated chemical reactivity, Nat. Commun. **13**, 7817 (2022).

[14] G. Arwas and C. Ciuti, Quantum electron transport controlled by cavity vacuum fields, Phys. Rev. B **107**, 045425 (2023).

[15] D. De Bernardis, T. Jaako, and P. Rabl, Cavity quantum electrodynamics in the nonperturbative regime, Phys. Rev. A **97**, 043820 (2018).

[16] M. Schuler, D. D. Bernardis, A. M. Läuchli, and P. Rabl, The vacua of dipolar cavity quantum electrodynamics, SciPost Phys. **9**, 066 (2020).

[17] Y. Ashida, A. İmamoğlu, J. Faist, D. Jaksch, A. Cavalleri, and E. Demler, Quantum electrodynamic control of matter: Cavity-enhanced ferroelectric phase transition, Phys. Rev. X **10**, 041027 (2020).

[18] G. M. Andolina, F. M. D. Pellegrino, V. Giovannetti, A. H. MacDonald, and M. Polini, Theory of photon condensation in a spatially varying electromagnetic field, Phys. Rev. B **102**, 125137 (2020).

[19] J. Román-Roche, F. Luis, and D. Zueco, Photon condensation and enhanced magnetism in cavity QED, Phys. Rev. Lett. **127**, 167201 (2021).

[20] F. Schlawin, A. Cavalleri, and D. Jaksch, Cavity-mediated electron-photon superconductivity, Phys. Rev. Lett. **122**, 133602 (2019).

[21] J. Hausinger and M. Grifoni, Dissipative dynamics of a biased qubit coupled to a harmonic oscillator: Analytical results beyond the rotating wave approximation, New J. Phys. **10**, 115015 (2008).

[22] A. Mercurio, V. Macrì, C. Gustin, S. Hughes, S. Savasta, and F. Nori, Regimes of cavity QED under incoherent excitation: From weak to deep strong coupling, Phys. Rev. Res. **4**, 023048 (2022).

[23] A. Settineri, V. Macrí, A. Ridolfo, O. Di Stefano, A. F. Kockum, F. Nori, and S. Savasta, Dissipation and thermal noise in hybrid quantum systems in the ultrastrong-coupling regime, Phys. Rev. A **98**, 053834 (2018).

[24] Q. Schaeverbeke, R. Avriller, T. Frederiksen, and F. Pistolesi, Single-photon emission mediated by single-electron tunneling in plasmonic nanojunctions, Phys. Rev. Lett. **123**, 246601 (2019).

[25] S. P. Kelly, A. M. Rey, and J. Marino, Effect of active photons on dynamical frustration in cavity QED, Phys. Rev. Lett. **126**, 133603 (2021).

[26] L. Magazzù, P. Forn-Díaz, and M. Grifoni, Transmission spectra of the driven, dissipative Rabi model in the ultrastrong-coupling regime, Phys. Rev. A **104**, 053711 (2021).

[27] S. P. Kelly, J. K. Thompson, A. M. Rey, and J. Marino, Resonant light enhances phase coherence in a cavity QED simulator of fermionic superfluidity, Phys. Rev. Res. **4**, L042032 (2022).

[28] Z.-H. Chen, H.-X. Che, Z.-K. Chen, C. Wang, and J. Ren, Tuning nonequilibrium heat current and two-photon statistics via composite qubit-resonator interaction, Phys. Rev. Res. **4**, 013152 (2022).

[29] C. Ciuti, G. Bastard, and I. Carusotto, Quantum vacuum properties of the intersubband cavity polariton field, Phys. Rev. B **72**, 115303 (2005).

[30] F. Schlawin, D. M. Kennes, and M. A. Sentef, Cavity quantum materials, Appl. Phys. Rev. **9**, 011312 (2022).

[31] J. Bloch, A. Cavalleri, V. Galitski, M. Hafezi, and A. Rubio, Strongly correlated electron–photon systems, Nature (London) **606**, 41 (2022).

[32] F. J. Garcia-Vidal, C. Ciuti, and T. W. Ebbesen, Manipulating matter by strong coupling to vacuum fields, Science **373**, eabd0336 (2021).

[33] G. M. Andolina, F. M. D. Pellegrino, V. Giovannetti, A. H. MacDonald, and M. Polini, Cavity quantum electrodynamics of strongly correlated electron systems: A no-go theorem for photon condensation, Phys. Rev. B **100**, 121109 (2019).

[34] J. Galego, C. Climent, F. J. Garcia-Vidal, and J. Feist, Cavity casimir-polder forces and their effects in ground-state chemical reactivity, Phys. Rev. X **9**, 021057 (2019).

[35] G. M. Andolina, A. De Pasquale, F. M. D. Pellegrino, I. Torre, F. H. L. Koppens, and M. Polini, Can deep sub-wavelength cavities induce Amperean superconductivity in a 2D material? arXiv:2210.10371 [cond-mat.supr-con].

[36] R. Sáez-Blázquez, D. de Bernardis, J. Feist, and P. Rabl, Can we observe nonperturbative vacuum shifts in cavity QED? Phys. Rev. Lett. **131**, 013602 (2023).

[37] J. Koch, F. von Oppen, and A. V. Andreev, Theory of the Franck-Condon blockade regime, Phys. Rev. B **74**, 205438 (2006).

[38] R. Leturcq, C. Stampfer, K. Inderbitzin, L. Durrer, C. Hierold, E. Mariani, M. G. Schultz, F. von Oppen, and K. Ensslin, Franck–Condon blockade in suspended carbon nanotube quantum dots, Nat. Phys. **5**, 327 (2009).

[39] Y. Cui, S. Tosoni, W.-D. Schneider, G. Pacchioni, N. Nilius, and H.-J. Freund, Phonon-mediated electron transport through CaO thin films, Phys. Rev. Lett. **114**, 016804 (2015).

[40] E. E. Vdovin, A. Mishchenko, M. T. Greenaway, M. J. Zhu, D. Ghazaryan, A. Misra, Y. Cao, S. V. Morozov, O. Makarovsky, T. M. Fromhold *et al.*, Phonon-assisted resonant tunneling of electrons in graphene–boron nitride transistors, Phys. Rev. Lett. **116**, 186603 (2016).

[41] T. Jaako, Z.-L. Xiang, J. J. Garcia-Ripoll, and P. Rabl, Ultrastrong-coupling phenomena beyond the Dicke model, Phys. Rev. A **94**, 033850 (2016).

[42] P. Forn-Díaz, L. Lamata, E. Rico, J. Kono, and E. Solano, Ultrastrong coupling regimes of light-matter interaction, Rev. Mod. Phys. **91**, 025005 (2019).

[43] A. Frisk Kockum, A. Miranowicz, S. De Liberato, S. Savasta, and F. Nori, Ultrastrong coupling between light and matter, Nat. Rev. Phys. **1**, 19 (2019).

[44] F. Yoshihara, S. Ashhab, T. Fuse, M. Bamba, and K. Semba, Hamiltonian of a flux qubit-LC oscillator circuit in the deep–strong-coupling regime, Sci. Rep. **12**, 6764 (2022).

[45] C. Gardiner and P. Zoller, *The Quantum World of Ultra-Cold Atoms and Light Book II: The Physics of Quantum-Optical Devices* (Imperial College Press, London, 2015).

[46] E. M. Kessler, G. Giedke, A. Imamoglu, S. F. Yelin, M. D. Lukin, and J. I. Cirac, Dissipative phase transition in a central spin system, Phys. Rev. A **86**, 012116 (2012).

[47] F. Minganti, A. Biella, N. Bartolo, and C. Ciuti, Spectral theory of Liouvillians for dissipative phase transitions, Phys. Rev. A **98**, 042118 (2018).

[48] K. Macieszczak, M. Guţă, I. Lesanovsky, and J. P. Garrahan, Towards a theory of metastability in open quantum dynamics, Phys. Rev. Lett. **116**, 240404 (2016).

[49] J. Johansson, P. Nation, and F. Nori, QuTiP 2: A Python framework for the dynamics of open quantum systems, Comput. Phys. Commun. **184**, 1234 (2013).

[50] T. Mori and T. Shirai, Resolving a discrepancy between Liouvillian gap and relaxation time in boundary-dissipated quantum many-body systems, Phys. Rev. Lett. **125**, 230604 (2020).

[51] F. Yoshihara, T. Fuse, S. Ashhab, K. Kakuyanagi, S. Saito, and K. Semba, Superconducting qubit–oscillator circuit beyond the ultrastrong-coupling regime, Nat. Phys. **13**, 44 (2017).

[52] P. Pilar, D. De Bernardis, and P. Rabl, Thermodynamics of ultrastrongly coupled light-matter systems, Quantum **4**, 335 (2020).

[53] D. Z. Rossatto, C. J. Villas-Bôas, M. Sanz, and E. Solano, Spectral classification of coupling regimes in the quantum Rabi model, Phys. Rev. A **96**, 013849 (2017).

[54] F. Beaudoin, J. M. Gambetta, and A. Blais, Dissipation and ultrastrong coupling in circuit QED, Phys. Rev. A **84**, 043832 (2011).

[55] E. K. Irish, Generalized rotating-wave approximation for arbitrarily large coupling, Phys. Rev. Lett. **99**, 173601 (2007).

[56] G. G. Claude Cohen-Tannoudji, Jacques Dupont-Roc, *Atom-Photon Interactions: Basic Processes and Applications*, Wiley Science Paperback Series (Wiley-VCH, Hoboken, 1998).

[57] K. E. Cahill and R. J. Glauber, Ordered expansions in boson amplitude operators, Phys. Rev. **177**, 1857 (1969).

[58] S. Ashhab and F. Nori, Qubit-oscillator systems in the ultrastrong-coupling regime and their potential for preparing nonclassical states, Phys. Rev. A **81**, 042311 (2010).

[59] L. Garziano, R. Stassi, V. Macrì, A. F. Kockum, S. Savasta, and F. Nori, Multiphoton quantum Rabi oscillations in ultrastrong cavity QED, Phys. Rev. A **92**, 063830 (2015).

[60] K. K. W. Ma and C. K. Law, Three-photon resonance and adiabatic passage in the large-detuning Rabi model, Phys. Rev. A **92**, 023842 (2015).

[61] T. Niemczyk, F. Deppe, H. Huebl, E. P. Menzel, F. Hocke, M. J. Schwarz, J. J. Garcia-Ripoll, D. Zueco, T. Hümmer, E. Solano *et al.*, Circuit quantum electrodynamics in the ultrastrong-coupling regime, Nat. Phys. **6**, 772 (2010).

[62] F. Yoshihara, T. Fuse, S. Ashhab, K. Kakuyanagi, S. Saito, and K. Semba, Characteristic spectra of circuit quantum electrodynamics systems from the ultrastrong- to the deep-strong-coupling regime, Phys. Rev. A **95**, 053824 (2017).

[63] S.-P. Wang, A. Ridolfo, T. Li, S. Savasta, F. Nori, Y. Nakamura, and J. Q. You, Probing the symmetry breaking of a light–matter system by an ancillary qubit, Nat. Commun. **14**, 4397 (2023).

[64] T. Holstein and H. Primakoff, Field dependence of the intrinsic domain magnetization of a ferromagnet, Phys. Rev. **58**, 1098 (1940).

[65] P. Rabl, Photon blockade effect in optomechanical systems, Phys. Rev. Lett. **107**, 063601 (2011).

[66] Y. Minoguchi, P. Kirton, and P. Rabl, Environment-induced Rabi oscillations in the optomechanical boson-boson model, arXiv:1904.02164 [quant-ph].

[67] P. Rabl, Cooling of mechanical motion with a two-level system: The high-temperature regime, Phys. Rev. B **82**, 165320 (2010).

[68] D. De Bernardis, P. Pilar, T. Jaako, S. De Liberato, and P. Rabl, Breakdown of gauge invariance in ultrastrong-coupling cavity QED, Phys. Rev. A **98**, 053819 (2018).

[69] O. Di Stefano, A. Settineri, V. Macrì, L. Garziano, R. Stassi, S. Savasta, and F. Nori, Resolution of gauge ambiguities in ultrastrong-coupling cavity quantum electrodynamics, Nat. Phys. **15**, 803 (2019).

[70] H. Breuer, F. Petruccione, and S. Petruccione, *The Theory of Open Quantum Systems* (Oxford University Press, Oxford, 2002).

[71] J. J. García-Ripoll, *Quantum Information and Quantum Optics with Superconducting Circuits* (Cambridge University Press, Cambridge, 2022).

[72] J. Dalibard, J. Dupont-Roc, and C. Cohen-Tannoudji, Vacuum fluctuations and radiation reaction: Identification of their respective contributions, J. Physique **43**, 1617 (1982).

[73] A. A. Clerk, M. H. Devoret, S. M. Girvin, F. Marquardt, and R. J. Schoelkopf, Introduction to quantum noise, measurement, and amplification, Rev. Mod. Phys. **82**, 1155 (2010).

Correction: A byline footnote along with its indicator was missing and has been inserted.